Università
Ca'Foscari
Venezia
Facoltà
di Scienze
Matematiche
Fisiche e Naturali

Corso di Laurea
in Chimica Industriale

Prova finale di Laurea

Synthesis, characterization and study of the catalytic and cytotoxic applications of supported palladium nanoparticles

Relatore
Ch. Prof. Alvise Benedetti

Corelatore
Ch. Prof. Santiago Gómez-Ruiz

Laureando
Francesco Gaballo
Matricola 805497

Anno Accademico
2012 / 2013

Index

1. Abstract

This thesis is divided into three different parts:

- Synthesis and characterization of materials based on supported palladium nanoparticles;
- Preliminary study of the catalytic activity of these materials in the Suzuki-Miyaura C-C coupling reactions;
- Preliminary study of the cytotoxic activity of the synthesized materials for their possible use as inhibitors of the reproduction of bone tumors.

Two different silica-based supports, namely SBA-15 and MSU-2, have been synthesized and characterized. In addition, commercial alumina has been used and characterized. These three surfaces have been loaded with different amounts of palladium nanoparticles by reactions in which different quantity of palladium precursor [$PdCl_2$(cod)] (cod = 1,5-cyclooctadiene) have been used in order to study their Pd-loading curve. The preparation of the Pd-support on SiO_2 or Al_2O_3 systems is based on the chemical reduction of the palladium compound in the presence of the surface and of a solvent (THF) which lead to the formation of palladium nanoparticles which remain impregnated on the corresponding surface. Using this syntheses method, the maximum amount of adsorbed palladium was 21.4% wt. on alumina, 12.8% wt. on SBA-15 and 4.46% on MSU-2. All the materials were characterized by gas physisorption (BET), X-ray diffraction (XRD), X-ray fluorescence (XRF) and electronic microscopy (SEM and TEM).

Pd-supported systems have been tested as catalysts in Suzuki-Miyaura reactions (SM), which is a typical catalytic reaction for the carbon-carbon coupling between organoboranes and aryl-, alkenyl- and / or alkynyl-halides to give symmetrical and / or asymmetrical biaryl compounds (products of great structural importance in organic and organometallic chemistry).

The two studied coupling reactions were:

- Reaction between 4-carboxyphenylboronic acid and 3-bromoanisole:

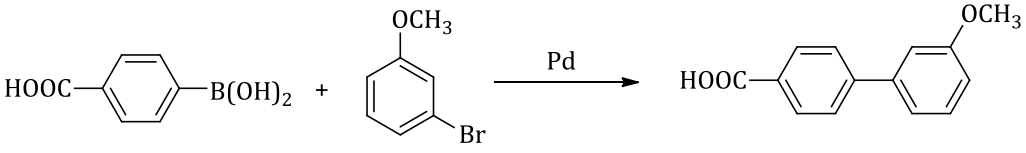

- Reaction between 4-carboxyphenylboronic acid and 2-bromopyridine:

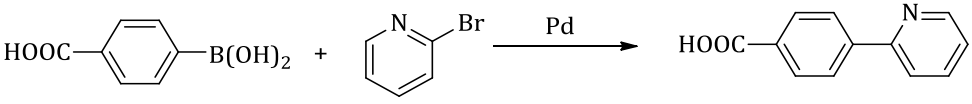

The catalytic activity of the Pd-supported systems in the described reactions has been quantified by gas chromatography (GC).

In the catalytic studies, the activity of the Pd-supported systems have been compared to that of the homogeneous commercial catalyst [$Pd(PPh_3)_4$], observing a lower activity of the heterogeneous catalysts compared to that of the reference compound. In addition, a study of the conversion of the corresponding arylhalide at different time periods has also been analyzed, observing that the reaction involving 3-bromoanisole is faster due to the higher reactivity of this compound. Furthermore, the catalytic results showed that the alumina-based catalysts lead to higher conversion of the halide than the silica-based materials (SBA-15 and MSU-2).

An additional study of the use of the catalyst for different cycles for all the employed catalysts has been carried out observing that, in a second cycle of catalysis, the catalytic activity of the silica-based materials decreases dramatically, while in the case of the alumina material AAL50, decreases moderately after the first cycle, but remain nearly constant from the second up to the fifth recycling cycle.

Finally, the study of the cytotoxic activity has been focused on the bare silica (SBA-15 and MSU-2) and on the Pd nanoparticles supported on SBA-15 and MSU-2 (Pd 15-15 and Pd 14-50), in order to get new insights on the anticancer mechanism of this class of materials, which may be useful for the future preparation of bone filling in patients with osteosarcomas or condroblastomas. The studied surfaces were analyzed to determine their *in vitro* cytotoxicity (in terms of M_{50} which is the quantity of material needed to inhibit normal cell growth by 50%) against anaplasic thyroid carcinoma cells (8505C), head and neck tumor cells (A253), lung carcinoma cells (A549) and colon carcinoma cells (DLD-1). All the materials show a dose-dependent cytotoxicity against all the studied cancer cells, except SBA-15 which showed no activity in the studied range (M_{50} > 1500 μg), however, not very clarifying conclusions about the cytotoxic nature of these materials could be obtain from the tests, because the cytotoxicity seems to depend on the amount of employed material, the amount of palladium, the studied cell type and the surface type.

2. Introduction

2.1. Palladium catalysts and carbon-carbon coupling reactions

Palladium is a very versatile metal in promoting or catalyzing many types of reactions: carbon-carbon coupling reactions, carbonylation of alkenes, dienes and haloaryl compounds, hydrogenations, reductions by hydrogen donors and hydrogenolysis of haloaryl compounds, for example.

There are many useful alternative reactions for the formation of new C-C bonds in the synthetic pathways for the preparation of biaryl compounds; namely, Suzuki-Miyaura, Heck, Kumada, Negishi, Stille and Sonogashira couplings, which are some highly exploited examples of this type of coupling reactions (Fig. 1).

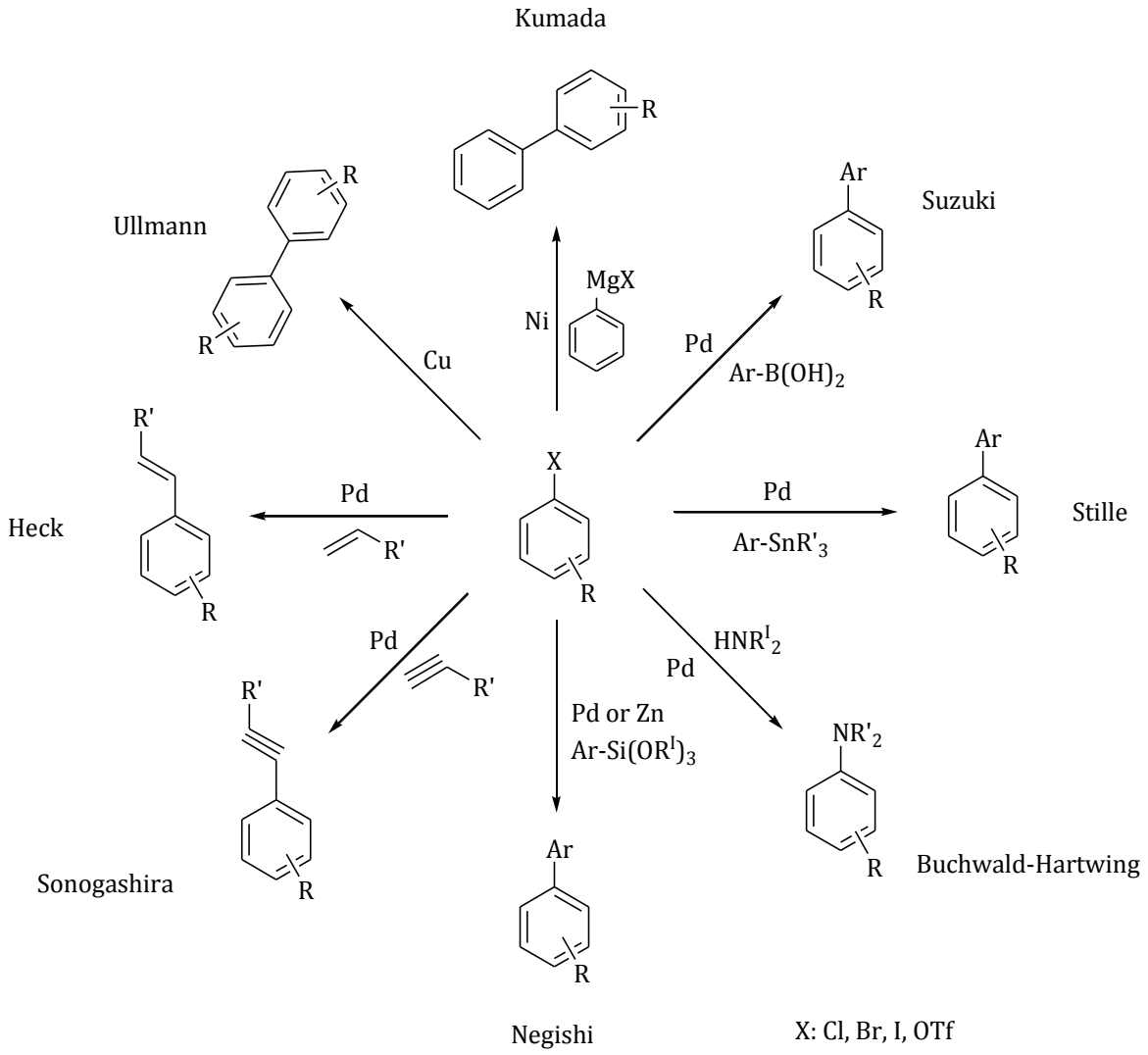

Fig. 1: Summary of catalytic C-C coupling reactions

C-C coupling reactions are widely exploited in industrial production and can be carried out in homogeneous and in heterogeneous phases. Due to the high demand of production of compounds which need a palladium-based catalyst, due to its importance in the industry of fine chemicals and the relatively high price of palladium, the use of heterogeneous catalysts is necessary to allow the recovering of the metal-containing active species.

Furthermore, the application of this reaction in the synthesis of pharmaceuticals makes the removal of the catalyst a must at the end of the reaction. Since FDA regulates the amount of all heavy metals that can be present in any product for human consumption a high number of reviews are devoted to the difficult task of the removal of Pd from organic products (MacQuarrie *et al*., 2010).

The simplest way to obtain a heterogeneous system consists in the deposition of the active species (metal and/or metal complexes) on a solid support that can be easily separated from the reaction mixture by filtration, decantation or centrifugation.

In this context, metal nanoparticles, due to its small size (less than 100 nm) and a relative high specific surface area, are a very attractive class of materials to be used in heterogeneous systems. However, due to the small size too, they are very mobile and are susceptible to agglomeration or sintering processes to form larger clusters of particles leading to a loss of the high surface area and, consequently, to a loss of catalytic activity.

The properties of nanoparticles-based catalyst, for a specific metallic system, depend on the support, the synthetic method and the particle size. The supporting material must be both thermally and chemically stable during the reaction process, and furthermore, should allow a good dispersion of the active phases (Barau *et al.*, 2008).

Taking into account all the previously explained reasons concerning the use of supported systems, the aim of the present work was the preparation of palladium nanoparticles supported on mesoporous silica and alumina in order to provide systems with advantages of heterogeneous catalysts, namely, easy to recover and to separate from the final products of the reaction. These systems should also avoid the agglomeration and/or leaching of the palladium nanoparticles from the supports which are the main reasons of the poor recyclability of some materials reported in literature (Barau *et al.*, 2008).

2.2. The Suzuki-Miyaura coupling reaction

The Suzuki-Miyaura reaction (SM), catalyzed by palladium compounds, is one of the most effective methods for the formation of new C-C bonds. It consists of a coupling reaction between organoboron compounds and aryl-, alkenyl- and/or alkynil- halides. This kind of reaction (Fig. 2) leads to the synthesis of

biaryles, which are elements of great structural importance in organic chemistry. Biaryl derivatives show a variety of physical and chemical properties, with applications in different fields such as pharmacy, polymers, liquid crystals, optically active ligands and ligands employed in catalysis, or as MOF's precursors (organometallic framework).

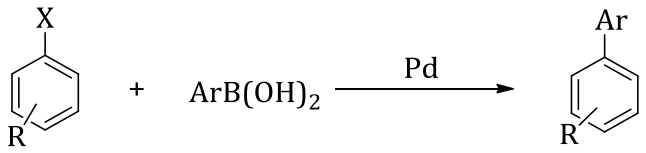

Fig. 2: Scheme of the Suzuki-Miyaura reaction

The first synthesis of biaryl derivatives through a cross-coupling reaction between an aryl halide and a boronic acid was achieved in 1981 by Suzuki and Miyaura (Fig. 3) and consisted in the condensation of phenylboronic acid with various aryl halides, employing $[Pd(PPh)_3]_4$ as catalyst. The reaction was subsequently improved using different reagents such as organoboron compounds and other substrates (alkenes, alkynes and aryl halides, for example).

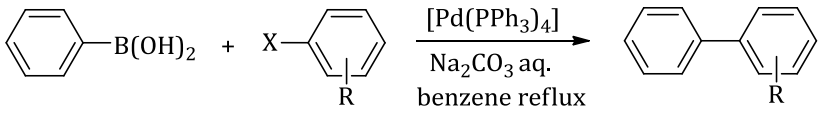

Fig. 3: First synthesis of biaryl derivatives through a cross-coupling reaction

Further optimizations of the reaction conditions by the change of some of its components have been studied. For example, other palladium-based catalysts such as $[PdCl_2(PPh_3)_2]$ or $Pd(OAc)_2$ have been used. In addition, the base has been changed to triethylamine, sodium or potassium bicarbonate, cesium or tantalum carbonate, as well as some of them combined with phase transfer catalysts as Bu_4NCl or crown ethers using various solvents or a combination of them.

The final product of these reactions may be symmetrical or asymmetrical since the Suzuki-Miyaura reaction allows the intermolecular coupling between two aryls with the same or different substituent. Thus, the cross-coupling reaction of organometallic reagents with organic halides proceeds through a three steps process in the presence of a base, which acts by activating the palladium complex favoring the formation of the species $ArPd(OR)L_2$, starting from $ArPdXL_2$ and thereby facilitating the transmetalation with organoboron compounds.

The first step (**a**) of the whole mechanism of the SM reaction , reported in (Fig. 4), is the oxidative addition of the organic halide to the metal center Pd(0), forming an organopalladium halide complex which

is often the rate determining step of the catalytic cycle. When the process implies the addition of 1-alkenyl, 1-alkynyl, allyl, benzyl, and aryl halides to a Pd(0) metallic center affords a stable *trans*-σ-palladium(II) complex, that proceeds with complete retention of configuration for alkenyl halides and with inversion of configuration for allylic and benzylic halides (Suzuki *et al*., 1995). Aryl and 1-alkenyl halides activated by the proximity of electron-withdrawing groups are more reactive to the oxidative addition than those with donating groups. The relative reactivity of different halo compounds decreases in the order I > OTf > Br >> Cl.

The second step (**b**) consists in the transmetalation between the species $[Ar^{I}B(OH)_3]^-$, formed *in situ* after the reaction between the organoboron reagent and the base, and the organopalladium compound Ar-Pd-OH. Since the C-B bond is nearly covalent, the coordination of a negatively charged base on the boron atom is necessary to activate the organoboron compound to the transmetalation reaction. The presence of a negatively charged base enhances the low nucleophilicity of the organic group attached to boron atom, forming the corresponding borate complex. This results in an improvement of the transmetalation rate. It has been reported that the cross-coupling reaction of arylboronic acids with aryl halides at pH = 7 - 8.5 is retarded relative to the reaction at pH = 9.5 – 11 (Suzuki *et al*., 1995). This reaction affords the formation of the diorganopalladium complex $Ar\text{-}Pd\text{-}Ar^{I}$.

The third and last stage (**c**) is the reductive elimination of the coupling product. Reductive elimination of organic partners $Ar\text{-}Ar^{I}$ leads again to the palladium(0) metallic centre.

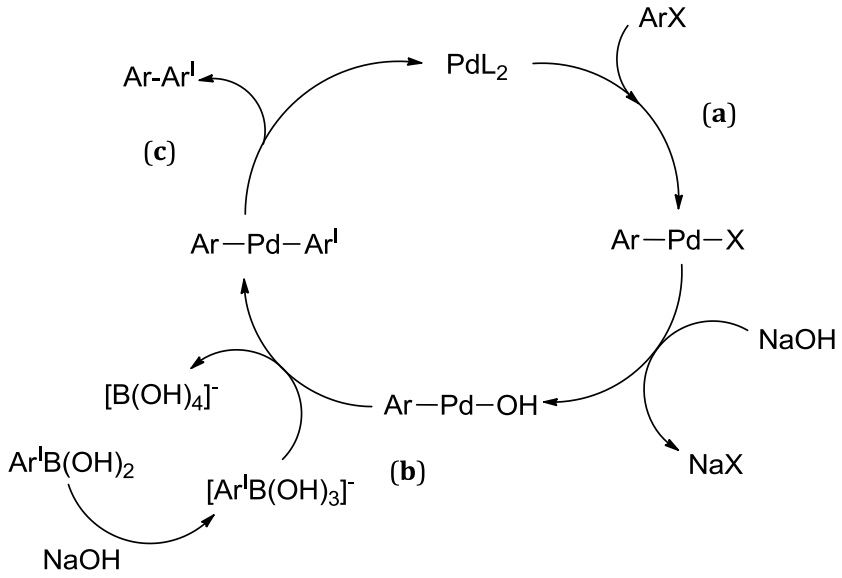

Fig. 4: Catalytic cycle of the Suzuki-Miyaura reaction

The reaction takes place directly from *cis*-$Ar\text{-}Pd\text{-}Ar^{I}$ complex and the *trans* complex reacts after its isomerization to the corresponding *cis*-complex (Fig. 5)

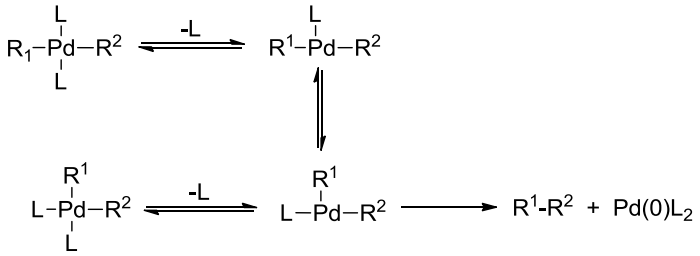

Fig. 5: Isomerization reaction of the *trans* complex

The order of reactivity, to form the new σ carbon-carbon bond, is diaryl derivative > (alkyl)aryl derivative > dialkyl derivative , suggesting participation of the π-orbital of the aryl group during the bond formation (Fig. 6) (Suzuki *et al*., 1995).

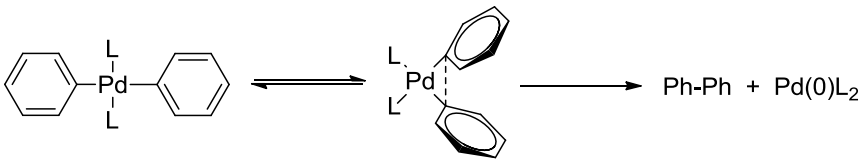

Fig. 6: Proposal for the participation of the π-orbital of aryl group during the bond formation

Although steric hindrance in this reaction is not the determining factor in the formation of substituted biaryl compounds, lower yields are obtained when *orto*- substituted arylboronic acids are used. For example, the reaction employing mesityl boronic acid proceeds slowly because of the steric hindrance during the transmetalation process. The addition of strong bases such as aqueous NaOH in benzene or DME, remarkably accelerates the coupling. On the other hand, the use of weak bases provides better results with less hindered arylboronic acids. The order of reactivity of these compounds corresponds to the strength of the base used in the reaction:

$$Ba(OH)_2 > NaOH > K_3PO_4 > Na_2CO_3 > NaHCO_3$$

However, even when there is not a large steric hindrance, the reaction performed in aqueous solution leads to the formation of secondary products due to a hydrolytic deboronation reaction. In addition to this process, the Suzuki-Miyaura reaction has two drawbacks (Pérez de Haro, 2002):

1. The presence of electron donating groups on the boronic acid increases the exchange of the aryl groups and the phosphine ligands to the metal center. This is an undesired reaction which can be suppressed maintaining the amount of employed catalyst to a minimum, using steric demanding trialkylphosphine, performing the reaction in solvents of low polarity or using catalysts without phosphine ligands;

2. When the cross coupling occurs very slowly, due to steric or electronic effects, it competes with the autocoupling of the aryl boronic acid.

However, the basic advantages of this reaction that have made SM one of the most used reactions to achieve the formation of a new carbon-carbon bond are the ease of synthesis, the mild reaction conditions and the low toxicity of the reagents, since boronic acids are less environmentally hazardous than other organometallic reagents. These features make the reaction suitable to be used in large scale synthesis of a high number of products (Kotha et al., 2002).

Furthermore, boronic reagents have several remarkable advantages compared to other organometallic derivatives, for example, tolerance to a wide range of functional groups (organic halides, carbonyl, etc.) and a very high reactivity. This is due in part to the electronegativity of the boron atom (2.0) which has a very close value to that of the electronegativity of carbon (2.5) and much greater than those of lithium, magnesium or most of the transition metals.

In homogeneous catalysis, $Pd(PPh_3)_4$ is the most commonly used catalyst, but $PdCl_2(PPh_3)_2$ and the mixture $Pd(OAc)_2$ / PPh_3 or other phosphine ligands are also efficient since they are stable to air and rapidly reduced to active Pd(0) complexes with organometallics or phosphines used for the cross-coupling reactions. Palladium atoms containing fewer than four phosphines ligands or bulky phosphines in their coordination sphere are, generally, highly reactive for the oxidative addition because of the rapid formation of coordinate unsaturated palladium species.

2.3. Nanoparticles supports

Metal nanoparticles have attracted much attention over the last decade due to potential modifications of their size, shape and activity. This makes them particularly interesting in a variety of applications including sensors, non-linear optics, medical dressings and catalysis (Budarin *et al*., 2007). The supporting material on which these nanoparticles are loaded has also received significant attention in the literature. The possibilities in the choice of solid supports in the synthesis of impregnated metal nanoparticles is very wide, ranging from organic polymers to various transition metal oxides, ordered mesoporous silicas and microporous zeolites. In recent years, hydroxyapatite has also received much attention as exploitable support for the synthesis of metal nanoparticles-based catalysts, for its use, for example, in aerobic oxidation of alcohols and in the Suzuki-Miyaura reaction obtaining very good yields of the final products (Jamwal *et al*., 2008). Budarin *et al*. used starch for the preparation of a porous support, finding that nanoparticle size distribution was controllable by the selection of the reaction solvent. The obtained material showed excellent catalytic activity in the cross coupling reaction and a very easy recyclability.

The most important factors to consider in the choice of a material to use as support are the following:

1. The material must present both thermal and chemical stability under the chosen reaction conditions.
2. The active sites on the support must be homogeneously dispersed and easily accessible, condition generally achieved with high surface areas (> 100 m^2/g) and mesoporous structures (pore size > 2 nm).

Mesoporous silicas were discovered in the early 1990s by scientists at Mobil Oil Company and by Kuroda and co-workers, in part as a response for the need of extending the applications of zeolites (Slowing *et al*., 2010). These interesting materials offer many of the features expected from an ideal support: a very large surface area (> 600 m^2/g), a narrow pore distribution (2 - 50 nm), high thermal and chemical stability, ready availability and easy chemical modification on the surface by anchoring catalytically active species.

Synthesis of mesoporous silica requires the participation of a templating agent, typically a surfactant in aqueous solution, which is either neutral or charged. The template directs the polymerization of silicates from a precursor, typically an ester of orthosilicic acid. The control of particle size and morphology of mesoporous silica can be attained in different ways, with the fundamental variables to control being the relative rates of hydrolysis and condensation of the silica source, and the magnitude of the interactions between the growing silica polymer and the assembled templates. These variables can be controlled by the choice of different templates, by the control of the pH of the synthesis, and by the use of co-solvents or additives. For example, the pore width can be adjusted by selecting surfactants with varying lengths of their hydrophobic chain (Slowing *et al*., 2010). The different size of the ordered structure of channels and pores leads to the differentiation between microporous materials (zeolites), mesoporous (MCM-41) and macroporous (amorphous silica) (Chun *et al*., 2009).

Due to their properties, mesoporous silicas are being exploited in the fields of catalysis, separation, ion exchange, molecular sieving and adsorption (Yuranov *et al*., 2002); they have also been proposed for environmental remediation upon functionalization with mercaptopropyl groups, which are able to remove heavy metals from water.

Functional groups and active species included in the support (thiol groups, organic ligands, metal nanoparticles, etc.) have great influence on the recyclability of the catalyst, on its activity and on the agglomeration of the nanoparticles. For example, the combination of the silica with an organic ligand has a synergic effect that increases the activity of the catalyst, preventing the agglomeration of the palladium nanoparticles and making the catalyst more durable (Babak *et al.,* 2006).

As already reported in literature (Lozano, 2005), alumina (Al_2O_3) presents the characteristics of thermal and chemical stability necessary to be used as support for heterogeneous catalysts; in the present work we used commercial alumina (Sigma-Aldrich) as support for the palladium nanoparticles.

The work presented here includes the synthesis, characterization and use of the following materials for catalytic purposes:

- SBA-15: mesoporous silica with planar hexagonal mesoporous structure, pore diameter between 2 and 30 nm, specific surface area around 700 m^2/g and pore volume up to 2.5 cm^3/g. This material is thermally stable, amorphous at the atomic level and contains micropores which interconnect the mesopores (Landau *et al.,* 2003);
- MSU-2: mesoporous silica with a sponge-like, porous and disorganized structure. The pore average size is about 3.5 nm, specific surface area up to 900 m^2/g pore volume up to 1.05 cm^3/g. (Pérez-Quintanilla et al., 2009)
- Alumina (Al_2O_3): aluminum-based amorphous material with specific surface area comprised between 50 and 250 m^2/g and pore volume between 0.1 and 1 cm^3/g (Lozano, 2005).

2.4. Synthesis of supported catalysts

As already underlined in the previous chapters, the properties and catalytic activity of supported catalysts, as well as the distribution and size of the supported species, are highly dependent on the support, methods of preparation and type and method of preparation of the noble metal. The incorporation of the palladium nanoparticles in the support system as well as the maximum effective loading of the metal for the material are two further aspects that must be considered in the nanoparticles preparation. Finally, the control of size and morphology of the nanoparticles during the catalytic reaction are two main aspects that have to be considered.

In addition, the presence of some functional groups on the surface of the supports may have an important role regarding these aspects, as well as in the catalytic activity or control the phenomenon of particle agglomeration (Barau *et al*., 2008).

Supported catalysts can be prepared in two ways: directly during surface synthesis or by post-synthesis treatment of the surface with a palladium precursor.

Post-synthesis functionalization of the surface offers various operating possibilities:

- Impregnation of a precursor of palladium (e.g. palladium acetate) followed by its reduction with various reducing agents (ethanol, $NaBH_4$, H_2, hydrazine) (Barau *et al*., 2008; Budarin *et al*., 2007)

- Ion exchange with metal precursors
- Adsorption of molecular cluster precursors
- Immobilization of metal complexes
- Photocatalytic reduction

All the cited methods are fast, but when the catalyst is reused, the activity decreases dramatically and their properties worsen due to structure collapsing (Yuranov *et al*., 2003). On the other hand, the kinetics of the metal reduction process, in most cases, is not easily controllable, green or simple to practice; so that the product also needs to be thoroughly washed and conditioned in order to remove the excess of reducing agent. This has led to a high number of study concerning improved preparation methods of metal nanoparticles. In particular, recently some research groups have employed glucose as an environmentally benign reducing agent to prepare well-dispersed Au and Ag nanoparticles (Budarin *et al*., 2007).

The method used for the synthesis of the nanoparticles on the support, inside the pores as well as on its external surface, influences their distribution and size in a decisive manner. For example, it has been found that if the synthesis of Pd nanoparticles occurs simultaneously to the synthesis of the silica support MCM-41, the nanoparticles remain anchored to the outer surface, while if they are introduced through a post-synthesis treatment they can be incorporated within the mesoporous structure of MCM-41 (Mastalir et al., 2006).

2.5. Anticancer studies

The term “cancer” refers to a group of about two hundred different diseases that have in common the uncontrolled cell division and growth. A neoplastic cell possesses the ability to invade the organ from which it was originated and overcome the boundaries both locally or by migration into the bloodstream and lymphatic systems, giving rise to metastasis.

The body is formed by a set of cells that periodically and regularly undergo replication, a phenomenon that allows maintaining the integrity and proper function of the organs. The process of cell division is controlled by mechanisms that regulate the timing of the phenomenon, when these mechanisms are altered, the cell itself and its descendants (or *daughters*) undergo uncontrolled division that produces hyperplasia or cancer.

All cancer cells, irrespective of the tissue of origin, have some common characteristics that result from the effect of multiple genetic alterations; the main characteristics are listed below:

- Self sufficiency of growth signals: while normal cells require growth factors to develop in culture, tumor cells generate their own growth signals and proliferate independently;

- Insensitivity to anti-growth signals: in contrast to normal cells that stop proliferating if they come in contact with growth inhibitors, cancer cells are insensitive to these factors;
- Resistance to apoptosis: normal cells in culture stop growing after a certain number of duplications, while tumor cells are immortal;
- Induction of angiogenesis: the formation of new blood vessels is essential because the tumor can continue being developed;
- Cell invasion and metastasis formation: allows the tumor to colonize distant sites where nutrients and space are more readily available.

Figure 7 summarizes the process of birth and development of a cancer.

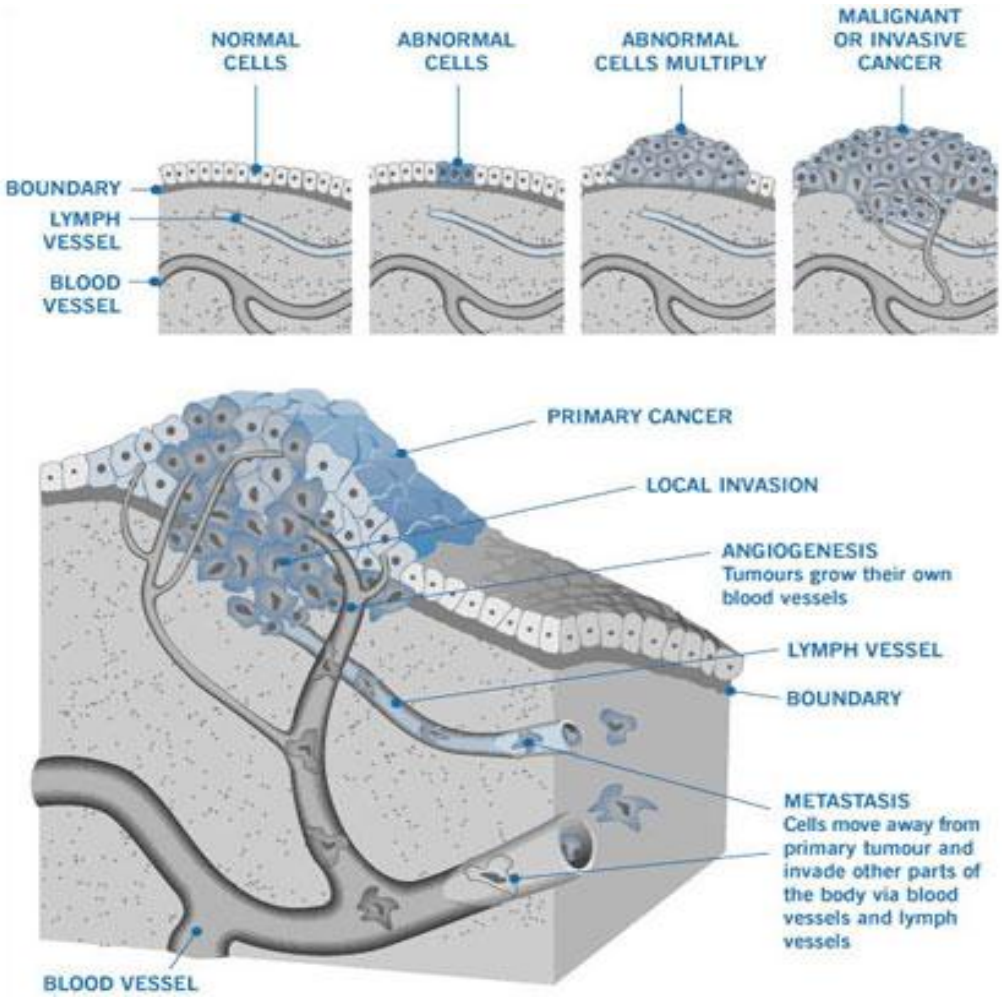

Fig. 7: Scheme of cancer birth and development

The process that leads to the formation of cancer is defined as carcinogenesis or initiator (UV light, sun radiation, asbestos, human papilloma virus, etc.), but this is not enough to cause the disease. However, their combination with a promoter (alcohol, tobacco, poor diet, etc.), allows the division process of the damaged cells becoming more active and destructive (Ahluwalia *et al.*, 1995). The degree of malignancy of

a tumor is a function of the aggressiveness of the cells that constitute it, which represents the characteristic which determines the degree of invasive capacity to other organs and / or tissues of the body.

In Western countries cancer is the second cause of death after cardiovascular diseases. Despite the progress of therapy has increased the number of healing and improved survival cases by reducing mortality, the incidence of cancer is rising in recent decades.

The number of cancer cases has rapidly and progressively increased due primarily to three factors:

1. The aging of the population, since its incidence increases with age.
2. The failure of anti-smoking campaigns, because lung cancer remains the leading cause of cancer death in the Western world, where its incidence continues increasing, especially among women, and is expanding in emerging countries.
3. Some changes in lifestyle, especially for breast and colon-rectal cancer.

Cancer is essentially an acquired genetic disease, because the transformation of normal cell into neoplasic cell requires the introduction of multiple genetic alterations. Rarely (once every million cell division) errors can occur during the replication of genes, resulting in a cell with an altered or damaged genetic code. A single defective cell does not cause cancer, however, it increases the probability, since the disease develops when a large number of mutated cells begin to replicate (Ahluwalia *et al*., 1995).

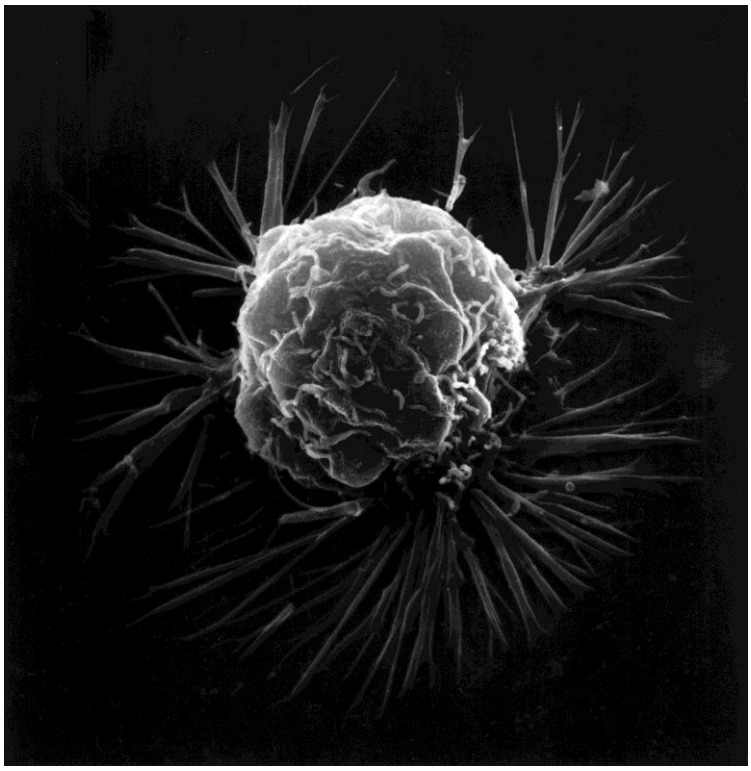

Fig. 8: SEM picture of a breast cancer cell

2.6. Types and treatments of bone cancer

In this work, we have studied the cytotoxicity of palladium supported nanoparticles, because previous studies in this topic have demonstrated that these materials are potentially useful as bone fillers for *in situ* treatment of bone tumors such as osteosarcoma or condroblastoma upon local implantations which may avoid recurrence of the tumor (Pérez-Quintanilla *et al*. 2009, Kaluderovic *et al*. 2010, García-Peñas *et al*. 2012, Sánchez-Muñoz *et al*. 2012). Thus, there are two types of bone tumors which are important to differentiate (Roncali et al., 2010):

- Primary bone cancer: is generated in the bone itself. Osteosarcoma is the most common, it is originated when bones are growing. Other primary bone cancers include chondrosarcoma (originating in cartilage) and fibrosarcoma (fibrous tissue). In addition, the cancerous tumor may be originated in the spinal cord (Ewing tumor and multiple myeloma).
- Secondary or metastatic bone cancer: is more common than primary and is due to a tumor which was originated in another area of the body. The most common are lung, breast, prostate, thyroid and kidneys. In general, metastasis occurs in the vertebrae, pelvis, ribs and skull. Possible treatments for bone cancer depend on the progress of the tumor and include surgery, radiotherapy, chemotherapy and complementary myeloablative therapy with stem cell support (Roncali et al., 2010).

Depending on the extent of the tumor in the bone, amputation may be required or surgery may be sufficient to eliminate the problem. In this case reconstructive surgery is used with the aim of recovering all or part of the functionality of the bone. In this type of surgery, there are possibilities for reproduction of the tumor in the same area, due to some remaining cancer cells in the bone. For this reason, the use of synthetic materials to prevent the reproduction of the tumor in the bone could be an interesting field for the development of further studies.

2.7. Cytotoxicity of metal nanoparticles and palladium compounds

Since we planned to study the use of palladium nanoparticles-based materials, we conducted a literature review regarding similar materials based on metal nanoparticles used in biological processes. Thus, it was determined that at present time there is no reference on the cytotoxicity of palladium nanoparticles. On the other side, several studies show the *in vitro* cytotoxicity of metal oxide nanoparticles, as well as some palladium complexes. This suggests the interesting possibilities that could provide the supported palladium nanoparticles in antineoplasic therapy.

Some metal nanoparticles presenting strong cytotoxic activity are ZnO, ZnO supported on SiO_2, CuO, NiO, Sb_2O_3, CoO, MoO_3, MgO; while metal nanoparticles of ZrO_2, Fe_2O_3, TiO_2, Al_2O_3 and CeO_2 showed low or even inexistent cytotoxic activity. Some of the properties of the nanoparticles that seems to influence the cytotoxic effects are particle size, surface area and the type and concentration of metal ions released into the medium. However, it was found that only the release of ions in the medium had a real important effect on the cytotoxicity. Furthermore, it is known that the cytotoxic nature is greater for soluble nanoparticles than that of the insoluble ones (Horie *et al*., 2012). The development of nanoparticles-based anticancer drugs begins to become important in the world of biomedicine, since they act only in cancer cells and have also fewer side effects. The mechanisms by which these nanoparticles exhibit anticancer activity are not fully understood (Vázquez *et al*., 2011), however, it is known that the key to understand the nanoparticles cytotoxicity is their small size, being lower than the size of a cell which allow them to penetrate the biological structures, altering their normal function.

In addition, the nanoparticles side effects on human health, beyond the chemistry, size, shape, charge, agglomeration state and electromagnetic properties, depend on individual factors such as genetic and existing disease (Vazquez *et al*., 2011), although further studies in this topic must be carried out in the future and could be of great interest.

On the other hand, dealing with the existing metal compounds with proven anticancer activity, the most known complex is cisplatin (*cis*-$[PtCl_2(NH_3)_2]$), a commercial anticancer drug used to treat various types of tumors, especially testicular, ovarian, and head and neck tumors. Its cytotoxic activity is based on the ability to form adducts with DNA, that are believed to be able to terminate replication and genes transcription (Abu-Surrah *et al*., 2002). Unfortunately, platinum causes serious side effects in the body, such as high tissue toxicity, including nephrotoxicity, neurotoxicity and ototoxicity, and also has a low water solubility.

In order to reduce these side-effects, a plausible alternative is the replacement of platinum with palladium, based on its high structural analogy and on their similar coordination chemistry. However, the *cis*-palladium complex (*cis*-$[PdCl_2(NH_3)_2]$) shows no antitumoral activity, due to the high reactivity of this compound (its hydrolysis reaction rate is one hundred times faster than their platinum analog). *Cis*-palladium rapidly dissociates in solution giving rise to highly reactive species that are unable to meet their drug targets. Therefore, to develop a palladium-based antitumor drug, the metal should be stabilized in some way (for example, with a chelate or a ligand and an appropriate leaving group) (Abu-Surrah *et al*., 2010).

For this reason, in the recent years, several palladium complexes presenting interesting antitumoral activity have been synthetized, showing fewer side effects that platinum compounds. Some of these

compounds exhibit comparable or even higher activities than cisplatin, carboplatin and oxaliplatin (Furlani *et al.,* 1998; Abu-Surrah *et al*., 2002; Zmejkovski *et al*., 2009; Divsalar *et al*., 2010; Gao *et al*., 2010; Ulukaya *et al*., 2011; Vazquez *et al*., 2011).

Thus, it seems clear that the modulation and the exchange of the ligands on the metal center Pd(II) has a great influence on the anticancer activity of these compounds. Nevertheless, there is little information regarding the cytotoxicity of palladium nanoparticles, which could be useful tools for the struggle against cancer, by analogy with other metal oxide nanoparticles having a high cytotoxic activity.

3. Experimental methods

3.1. General working conditions

Most of the experimental work has been performed using Schlenk tubes under inert nitrogen atmosphere (N_2 type B50: O_2 < 2 ppm, H_2O < 3 ppm, C_nH_m < 0.5 ppm, supplied by Air Liquide) to prevent water adsorption; a part of the experimental work has been performed in a dry box (model MBraun MB-OX-SEA), where the concentration of water and oxygen is less than 1 ppm.

Tetraethylorthosilicate (TEOS) 98%, poly(ethylene glycol)-block-poly(propylene glycol)-block-poly(ethylene glycol) (P123), Tergitol® NP-9, 4-carboxyphenylboronic acid, 2-bromopyridine 99%, potassium carbonate >99%, Al_2O_3, $PdCl_2$ and 1,5-cyclooctadiene were purchased all from Sigma-Aldrich, while 3-bromoanisole 98% was purchased from Alfa Aesar. All the chemicals were used as purchased, without further purification.

Water (resistence 18.2 MΩ cm) used in the preparation of materials was obtained from a Millipore Milli-Q-System (Billerica, MA, USA).

All the solvents employed were purchased from Carlo Erba and were purified according with existing literature (Perrin *et al.,* 1980), recovered by distillation and stored under nitrogen in Schlenk tubes provided with 4 Å molecular sieves.

3.2. Support synthesis and loading

Three different supports, MSU-2, SBA-15 and alumina (Al_2O_3), have been used and loaded with palladium nanoparticles, obtained by reduction of the precursor [$PdCl_2$(cod)]. MSU-2 and SBA-15 have been synthesized according to procedures described in literature; Al_2O_3 has been purchased from Sigma-Aldrich.

3.2.1. Synthesis of MSU-2

The synthesis of MSU-2 was carried out using the experimental procedure reported by Pérez-Quintanilla *et al.* (2009).

Tergitol® (78.135 g, 0.103 mol) was added in a two-necked flask containing 1562.5 mL of stirring Milli-Q water. After the complete dissolution of Tergitol®, TEOS (52.0 g, 0.250 mol) was added dropwise to the solution. After 30 minutes, stirring was stopped and the solution was left ageing for 20 hours; the solution slowly turned to a white suspension. After the ageing process, stirring was set at 800 rpm and 26 mL of NaF 0.24 M solution were added dropwise to the flask. Afterwards, temperature was raised at 55°C and the solution was stirred for additional 48 hours. Subsequently, the solution was filtered using a gooch filter

connected to a vacuum line; the white solid was abundantly washed with Milli-Q water, in order to eliminate all the soluble impurities and the remaining surfactant. After washing, a drying and a calcination process were carried out in a muffle oven, using the following temperature program:

$$30°C \xrightarrow{1°C/min} 100°C \xrightarrow{4\ hours} 100°C \xrightarrow{1°C/min} 600°C \xrightarrow{20\ hours} 600°C \xrightarrow{-2°C/min} 30°C$$

After the drying/calcination process, 15.08 g of a fine white powder of MSU-2 were obtained.

3.2.2. Synthesis of SBA-15

The synthesis of SBA-15 was carried out using the experimental procedure reported by by Zhao *et al.* (1998).

TEOS 98% aqueous solution (102 g, 0.480 mol) was added dropwise to a stirring solution containing the Pluronic 123 surfactant (48.4 g), 360 mL of Milli-Q water and 1342 mL of HCl 2 M at 35 °C and 1000 rpm. After the TEOS addition, the reaction was left under stirring (at 1000 rpm) and 35 °C for 20 hours. During this time, a white solid was formed in the reaction solution and after the reaction period the was increased to 80°C and the stirring stopped, for 24 hours, in order to complete the ageing process. Afterwards, the solution was filtered in a gooch filter connected to vacuum line and the resulting white solid was abundantly washed with Milli-Q water, in order to eliminate soluble impurities and the remaining surfactant. After washing, a drying and a calcination process were carried out in a muffle oven, using the following temperature program:

$$30°C \xrightarrow{1°C/min} 90°C \xrightarrow{6\ hours} 90°C \xrightarrow{1°C/min} 500°C \xrightarrow{24\ hours} 500°C \xrightarrow{-2°C/min} 25°C$$

After the drying/calcination process, 29.170 g of fine white powder of SBA-15 were obtained.

3.2.3. Loading of the synthetized supports

3.2.3.1. Synthesis of Pd nanoparticles precursor: [$PdCl_2$(cod)]

The synthesis of [$PdCl_2$(cod)] proceeds through two reactions, using $PdCl_2$ as palladium source:

$$PdCl_2 + HCl_{(concentrated)} \longrightarrow H_2PdCl_4$$

$$H_2PdCl_4 + cod \longrightarrow [PdCl_2(cod)] + 2\ HCl \qquad cod = 1,5\text{-cyclooctadiene}$$

$PdCl_2$ (3.05 g, 17.2 mmol) was dissolved in 8 mL of concentrated HCl. The cool solution was diluted with 250 ml of absolute ethanol and filtered through a filter paper; the residue and filter paper were then

washed with 40 mL of ethanol. After this step, 1,5-cyclooctadiene (5.0 mL, 40.7 mmol) was added to the resulting solution under stirring, the solution turned then from brown to deep yellow and the solid product precipitated immediately. The reaction was stirred for other additional 15 minutes and then filtered and the yellow solid product was washed with 60 mL (3 x 20 mL) of diethylether. The final product was dried under vacuum overnight to obtain 4.8 g (16.8 mmol) of [$PdCl_2$(cod)] as a yellow solid (yield: 98%).

3.2.3.2. Surface activation

Before the loading reactions, the surface of the materials needs to be previously activated. The activation consists in the dehydration and elimination of the physisorbed solvents on the hydroxyl functional groups present on the surface (fig. 9).

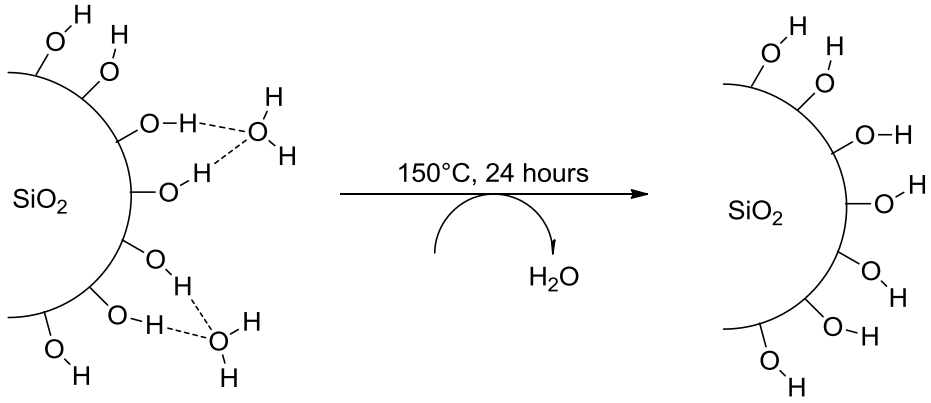

Fig. 9: Activation of the silica surface

The process was carried by the treatment of the corresponding surface under vacuum conditions for 24 hours at 150°C.

3.2.3.3. Surface loading

Three different palladium nanoparticles based materials have been synthetized by functionalization of three type of surfaces, SBA-15, MSU-2 and Al_2O_3, through the reduction of the palladium precursor [$PdCl_2$(cod)] starting from different palladium amounts. Table 1 shows the quantity of palladium and surfaces employed.

For the calculation of the [$PdCl_2$(cod)] mass to be used for obtaining the Pd amount on the surface, equation (1) has been used.

$$[PdCl_2(cod)], (mg) = m\,Pd\ (mg) \cdot \frac{MW_{[PdCl_2(cod)]}}{MW_{Pd}} \qquad (1)$$

Table 1: Pd relations in the loading reactions

Starting Pd, %	Support, g	$[PdCl_2(cod)]$, mg
1	1.0	27.0
2	1.0	54.0
5	0.5	67.5
10	0.5	135.0
20	0.5	270.0
50	0.5	675.0

The general procedure carried out for the preparation of the materials was as follows: In a dry box, the corresponding amount of the surface and $[PdCl_2(cod)]$ were introduced into a Schlenk tube and 30 mL of tetrahydrofurane (THF) were subsequently added under inert atmosphere. The reaction mixture was then heated at 80°C and stirred for 48 hours. The reaction conditions were determined in previous studies of our research group, in which syntheses were carried out at different temperatures, reaction times and solvents, proving that the greater efficacy was obtained using THF as solvent, at 80°C and after 48 hours of reaction. Subsequently, the loaded support was filtered on a gooch filter and washed several times with solvents of increasing volatility (2 x 50 mL each), namely THF, toluene, hexane and ether. Finally, the material was dried under vacuum for 12 hours to eliminate all traces of solvents. This procedure has been repeated for each starting amount of palladium and for all the studied supports (MSU-2, SBA-15 and alumina).

3.3. Catalytic tests

3.3.1. Preliminary tests

The catalytic activity of the synthetized materials in the Suzuki-Miyaura coupling reactions have been preliminary compared to the activity of a homogeneous Pd catalyst, $[Pd(PPh_3)_4]$, purchased from Sigma-Aldrich.

The following reactions have been studied:

- Reaction between 3-bromoanisole and 4-carboxyphenylboronic acid:

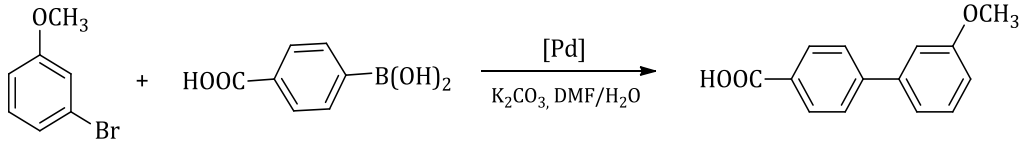

- Reaction between 2-bromopyridine and 4-carboxyphenylboronic acid:

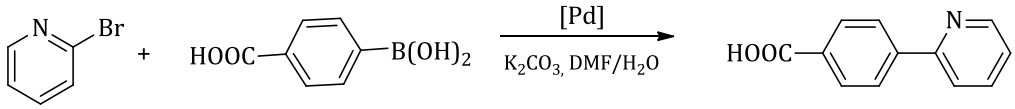

The reactions have been performed maintaining some common conditions, in order to facilitate a subsequent analysis of the results:

- Limiting reagent was the halide derivative;
- Molar ratio between the boronic acid and the halide was 1.2 to 0.8;
- Molar ratio between the base (K_2CO_3) and the halide was 2 to 1;
- Catalyst amount was maintained at 50 mg.

The experimental procedure has been the same for both reactions, using the corresponding halide for each case. Degassed solvents and a nitrogen atmosphere were used in the reaction to achieve higher final conversions (Trilla *et al.*, 2008).

The general procedure carried out for the catalytic reactions was as follows: A three-necked flask was filled with boronic acid (0.2 g, 1.2 mmol), K_2CO_3 (0.22 g, 1.6 mmol) and Pd catalyst and three cycles vacuum/N_2 (10 minutes/1 minute) under stirring were applied to eliminate oxygen from the reaction atmosphere. Paralelly, the solvent (DMF/H_2O 95/5, 10 mL) and the halide compound were mixed under nitrogen in a Schlenk tube, bubbling N_2 inside the solution for 10 minutes to eliminate dissolved oxygen. Subsequently, this mixture was transferred to the three-necked flask with the solide mixture under N_2. The suspension was then heated to the corresponding temperature (using a condenser in the case of refluxing conditions) and stirred for 24 hours. The tests were carried out in duplicate, the reported results are the average of the two obtained results.

After this time, the solution was cooled to room temperature and transferred inside a flask and the solvent was eliminated using a rotavapor. The purification of the product was performed using a chromatographic column, charged with silica gel and the suitable eluent to separate the reaction product was chosen on the basis of tests carried out on thin layer chromatography (TLC).

For reaction n° 1 (3-bromoanisole + 4-carboxyphenylboronic acid) dichloromethane/toluene (9/1) has been used as eluent solution. The solution containing the product was dried by elimination of the solvent with a rotavapor and the light yellow solid obtained was dried overnight at 60°C under vacuum. The product was characterized by ^{1}H-NMR analysis, using D_2O as solvent. ^{1}H-NMR (400 MHz, D_2O, 25°C): δ = 4.60 (s, 3H, -OC*H*$_3$), 6.84, 7.07, 7.14 and 7.27 (m, 1H each, H of anisole ring), 7.75 and 7.52 (d, 2H each, H of 4-carboxyphenyl ring), COOH (not observed due to exchange with D of D_2O).

For reaction n° 2 (2-bromopyridine + 4-carboxyphenylboronic acid) acetonitrile/water (7/3) has been used as eluent solution. The solution containing the product was dried by elimination of the solvent with a rotavapor and the orange solid obtained was dried at 60°C under vacuum overnight. The product was characterized by ^{1}H-NMR analysis, using d_6-DMSO as solvent. ^{1}H-NMR (400 MHz, d_6-DMSO, 25°C): δ = 7.29 (m, 1H, Pyr), 7.86 (m, 2H, Pyr), 7.93 (m, 1H, Pyr), 7.78 and 7.69 (d, 2H each, H of 4-carboxyphenyl ring), 10.00 (br, 1H, COOH).

The technique employed to quantitatively analyze the conversion of 3-bromoanisole and to recognize the reaction product was gas chromatography (GC).

The kinetics or the conversion of the different reactions was determined by following the variation of the concentration of the 3-bromoanisole in solution. The boronic acid, being more polar, is affected by interactions with the stationary phase of the chromatographic column more than the halide, thus, the quantification is more complicated due to the appearance of broader peaks difficult to integrate. To follow the changes of the halide concentration, an internal standard compound (1-octanol) has been used. Comparing the areas relating to the signals of the halo compound and the internal standard, the concentration of the halide can be determined with accuracy. The chosen internal standard was 1-octanol (100 ppm), being this compound inert with reagents and products and having a retention time different from the others compounds. The solution samples to be analyzed have been diluted in the ratio 1:50 in order to adjust the concentration of reactants and products to the range of linearity of the calibration curve. The calibration curve was prepared using concentration of halide in the range 0-500 ppm for both reactions. The calibration linear plot for 3-bromoanisole is presented in fig. 10.

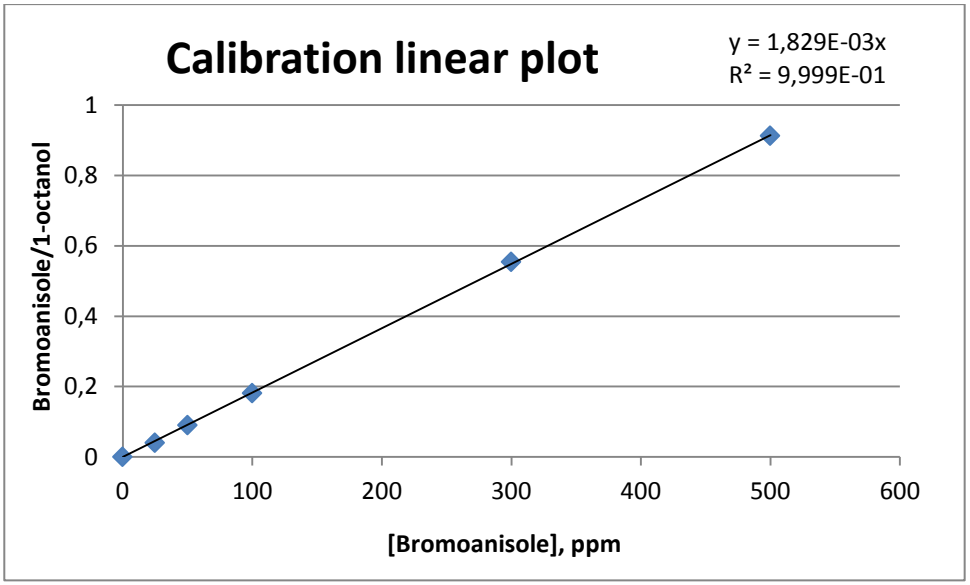

Fig. 10: Calibration linear plot for 3-bromoanisole

In the GC analysis the following conditions of time and temperature have been used:

- Injector temperature: 240°C;
- Detector temperature: 250°C;
- Temperature program (oven): 130°C (10 min); from 130°C to 210°C (with a ramp of 20°C/min), 210°C (10 min).

Operating with these conditions and using a column of 15 meters of polyethylenglycol, the retention times of the chemical species in solution were:

- DMF: 3.5 min.
- 1-octanol: 6.5 min.
- 3-bromoanisole: 12.0 min.
- 4-carboxyphenylboronic acid: 16.7 min.
- Product: 20.0 min.

3.3.2. Detailed tests

Two different tests have been performed in order to:

- quantify the conversion of the 3-bromoanisole in the reaction n° 1 (3-bromoanisole + 4-carboxyphenylboronic acid) using different amount of catalyst and
- determine the loss of activity of the catalysts in the first catalytic cycle.

The conversion studies were carried out using 15 mg and 5 mg of each of the following catalysts: AAL50, AAL20, Pd 14-50 and Pd 15-15. Conversion experiments were performed in a single-neck Schlenk tube. Solution samples were collected and analyzed at the beginning and at the end of the reaction time.

For these tests, the experimental procedure was as follows: In a Schlenk tube, 4-carboxyphenylboronic acid (9.95 mg, 0.06 mmol), K_2CO_3 (11.05 mg, 0.08 mmol) and Pd catalyst (15 mg or 5 mg) were treated with three cycles vacuum/N_2 (10 minutes/1 minute) under stirring to eliminate oxygen and subsequently a solution of 3-bromoanisole (7.5 mg, 0.04 mmol) in DMF/H_2O 95/5, (15 mL, with a previous N_2 bubbling of 10 minutes) was added to the mixture. The suspension was then heated to 70°C and stirred for 48 hours. Dilutions 1:10 of the samples were analyzed by GC.

The use of the catalysts for different cycles has been carried out using the same experimental procedure but using 15 mg of recycled catalyst. In the case of AAL 50 the study was more exhaustive and

was tested in up to five catalytic cycles in a row. In this case, the reaction were performed on a larger scale, but using the same experimental conditions. The tests started from a higher amount of catalyst in order to be able to carry out five catalytic cycles, due to some losses of the catalyst during filtration. The final amount of reactants used in the different recyclability tests are shown in Table 2.

Table 2. Final amount of reactants used in the different recyclability tests

	Cycle n°1	Cycle n°2	Cycle n°3	Cycle n°4	Cycle n°5
3-bromoanisole	327.2 mg	310.9 mg	294.5 mg	278.2 mg	261.8 mg
4-carboxyphenylboronic acid	432.8 mg	412.9 mg	390.5 mg	368.1 mg	348.2 mg
K_2CO_3	480.9 mg	458.8 mg	434.0 mg	409.1 mg	387.0 mg
DMF/H_2O 95/5	65 mL	62 mL	59 mL	55 mL	52 mL
Catalyst (AAL50)	1.0 g	0.95 g	0.9 g	0.85 g	0.80 g

3.4. Cytotoxicity in vitro studies

Cellular cytotoxicity is the capacity to interact with other cells and damage or destroy them, either *in vivo* or *in vitro*. These tests have been carried out at the Biozentrum of the Martin Luther University of Halle-Wittenberg, Halle (Saale), Germany, under the supervision of Prof. Dr. Goran Kaluderovic and Dr. Reinhard Paschke.

3.4.1. Drug preparation

Stock suspensions of the bare supports and the palladium-supported materials were prepared in dimethylsulfoxyde (DMSO) at a proportion of 20 mg/mL and diluted by nutrient medium to various working concentrations.

In all cases, nutrient medium was RPMI-1640 (PAA Laboratories) supplemented with 10% fetal bovine serum (Biochrom AG) and 1% penicillin/streptomycin (PAA Laboratories). Fetal bovine serum has an undefined composition and contains necessary growth factors for cells cultivation, whereas penicillin/streptomycin prevents microorganisms growth around cells.

3.4.2. Cell culture

The cell lines used in the present work, 8505 C (anaplasic thyroid cancer), A253 (head and neck cancer), A549 (lung carcinoma), A2780 (ovarian cancer) and DLD-1 (colon cancer) were kindly provided by Dr. Thomas Mueller, Department of Hematology/Oncology, Martin Luther University of Halle-Wittenberg, Halle (Saale), Germany.

Cultures were maintained as monolayer in RPMI-1640 (PAA Laboratories, Pasching, Germany) supplemented with 10% heat inactivated fetal bovine serum (Biochrom AG, Berlin, Germany) and penicillin/streptomycin (PAA Laboratories) at 37°C in a humidified atmosphere of 5% (v/v) CO_2.

3.4.3. Cytotoxicity assay

The cytotoxic activities of the materials were evaluated using the sulforhodamine-B (SRB, Sigma Aldrich) microculture colorimetric assay (Skehan *et al*., 1990).

Cancer cells were seeded into 96-well plates and kept under incubation for 24 hours. After 24 hours, the cells were treated with various suspensions of increasing concentration of the materials to be analyzed, for 96 hours. The final concentration of DMSO never exceeded 0.5% to be non-toxic to the corresponding studied cells.

The percentages of surviving cells were determined 96 hours after the beginning of drug exposure. After 96 hours treatment, the supernatant medium from the 96 well plates was eliminated and the cells were fixed with a 10% solution of trichloroacetic acid (TCA). After fixation, the cells were washed in a strip washer. The washing was carried out four times with water using alternate dispensing and aspiration procedures.

The plates were then dyed with 100 µL of 0.4% SRB for about 45 minutes. After dying, the plates were again washed to remove the dye with 1% acetic acid and dried to air overnight. 100 µL of 10 mM tris-hydroxymethylaminoethane (TRIS) were added to each well of the plate and absorbance was measured at 570 nm using a 96-well plate reader (Tecan Spectra, Crailsheim, Germany). The M_{50} value was estimated from the dose-response curves and was defined as the quantity (in µg) of the material at which 50% cell inhibition was observed.

3.5. Characterization of the materials

3.5.1. N_2 adsorption-desorption analysis

N_2 gas adsorption-desorption isotherms at 77 K were recorded using a Micromeritics ASAP 2020 instrument. The samples were degassed for 12 hours under vacuum ($p < 10^{-2}$ Pa) and subsequently analyzed. The specific surface area was calculated employing the BET method. The pore size distribution and the mesopore volume were calculated from the adsorption branch of the N_2 physisorption isotherms and the Barret-Joyner-Halenda (BJH) formula.

3.5.2. XRD and XRF analysis

The X-ray diffraction (XRD) spectra were performed on a Phillips PW3040/00 X'Pert powder diffractometer, at 45 kV and 40 mA, using the Cu-K_α line (λ = 1.5418 Å) in the 2θ angle range of 0.5 – 90°. X-ray fluorescence (XRF) analyses were performed using the same instrument.

3.5.3. SEM analysis

Scanning electron microscopy (SEM) was used to evaluate the size and the shape of the particles of the materials (morphology characterization). The analyses were carried out using a scanning electronic microscope Phillips XL30 ESEM; the samples was treated with a sputtering method with the following parameters: sputter time 100 s, sputter corrent 30 mA, film thickness 20 nm, using a sputter coater BAL-TEC SCD 005.

3.5.4. TEM analysis

Transmission electron microscopy (TEM) was applied to characterize the mesoporous structure of the materials and the location and conformation of Pd nanoparticles supported on the catalysts. A transmission electronic microscope Phillips Tecnai 20 with 200 kV field emission gun and resolution of 0.27 nm was used.

3.5.5. NMR analysis

Nuclear magnetic resonance (NMR) spectra were obtained with a Varian Mercury FT-400 spectrometer, operating at a frequence of 400 MHz for the ^{1}H spectra.

3.5.6. GC analysis

Gas chromatography (GC) analysis of the reaction mixtures was followed using a gas chromatographer Varian Chromopack CP-3380, provided with a Forte GC Capillary column, model BP20 (polyethylenglicol) (15 meters), using N_2 as carrier.

4. Results and discussion

4.1. Support synthesis, loading and characterization

The synthesis of the two silica-based mesoporous supports SBA-15 and MSU-2 was carried out using the reported methods of Zhao *et al.* (1998) and Pérez-Quintanilla *et al.* (2009), respectively; Al_2O_3 was purchased from Aldrich.

The supporting materials were then treated with increasing amounts of [$PdCl_2$(cod)] in THF during 48 hours to give systems which consist of the corresponding support and impregnated palladium nanoparticles. Under the proposed reaction conditions [$PdCl_2$(cod)] is reduced to form palladium nanoparticles that remain adsorbed in the material. The mechanism of the reaction is not completely clear, however, it seems that THF acts as direct reducing agent (together with the hydroxyl groups at the surface of the materials) of the palladium(II) complex to Pd0 in form of palladium nanoparticles which accumulate in the pores of the corresponding materials or remain impregnated in the external surface of the supports.

All the synthesized materials were characterized by different methods, and their catalytic application in the Suzuki-Miyaura cross-coupling reaction and as cytotoxic agents against cancer cells have been studied.

4.1.1. Gas physisorption analysis

The studied materials were characterized with a porosimeter by N_2 adsorption-desorption isotherms (BET method), which allowed to determine the specific surface area of the materials, the average pore diameter and the pore volume. Figures 11, 12 and 13 illustrate the adsorption-desorption isotherms of SBA-15, MSU-2 and alumina, respectively.

According to the IUPAC classification, SBA-15 presents a physisorption type IV isotherm, typical of mesoporous systems, with a type H1 hysteresis loop, which typically features a two-dimensional *P6mm* structure formed by open cylindrical mesopores (Sing *et al.*, 1984). MSU-2 shows a physisorption type IV isotherm with a type H4 hysteresis loop typical of some disordered mesoporous systems (Sing *et al.*, 1984).

In both isotherms, two defined inflexion points are observed. The first point (at a relative pressure of 0.1 in SBA-15 and 0.2 in MSU-2) is associated to the end of the monolayer adsorption of the adsorptive gas and the beginning of multilayer adsorption; while the second point (at a relative pressure of ca. 0.6 in SBA-15 and 0.35 in MSU-2) is associated to the capillary condensation of the adsorptive gas within the mesoporous structure of the analyzed materials.

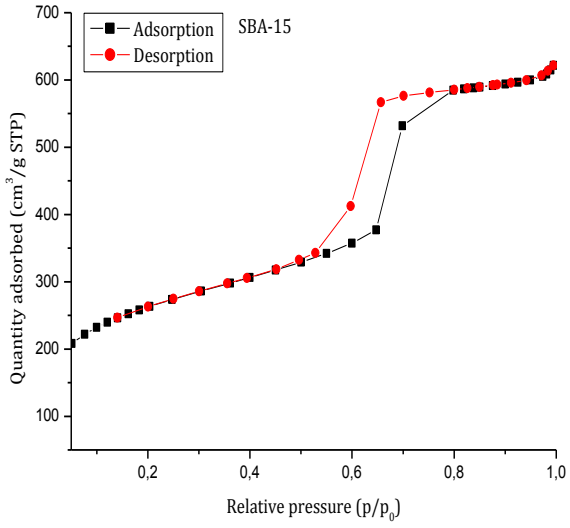

Fig. 11: Adsorption-desorption isotherms of SBA-15

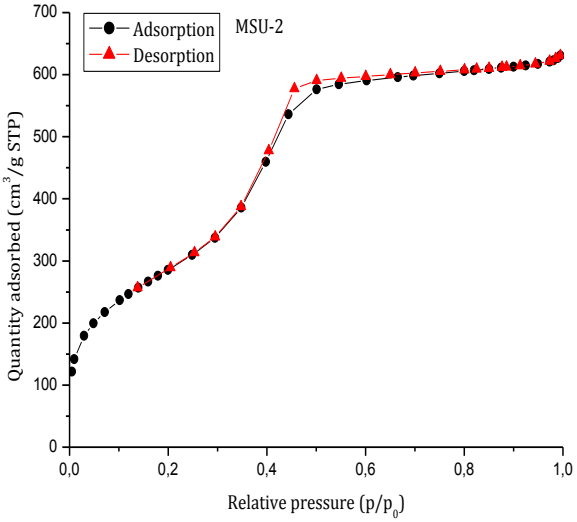

Fig. 12: Adsorption-desorption isotherms of MSU-2

Alumina presents a reversible type II isotherm, typically associated with non-porous or macroporous adsorbents, with a type H3 hysteresis loop. This surface is not mesoporous and presents a system of macro or micropores which are neither defined nor homogeneous.

Comparing the textural properties of silica-based materials, reported in the following tables, it can easily see that MSU-2 shows a greater specific surface area, a smaller pore diameter and a greater pore volume than SBA-15. All the obtained parameters are in the range of reported mesoporous silica (Zhao *et al.* (1998) and Pérez-Quintanilla *et al.* (2009)).

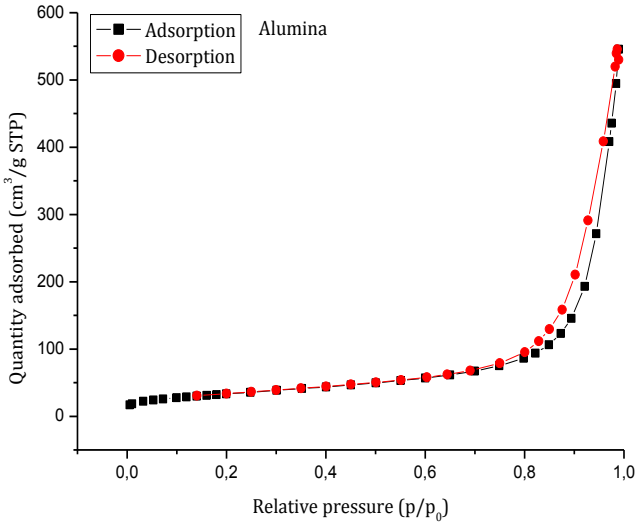

Fig. 13: Adsorption-desorption isotherm of alumina

Regarding the pore size distribution, a narrow distribution has been observed for SBA-15 and MSU-2 as it is confirmed by Figures 14 and 15. The narrow and defined peaks are typical of a homogeneous pore diameter distribution.

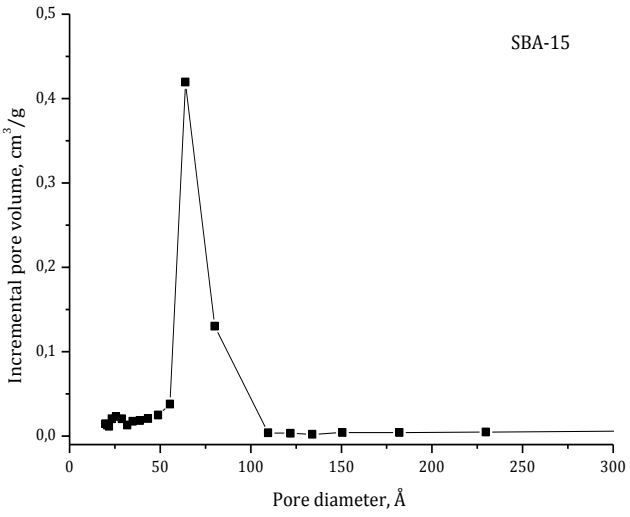

Fig. 14: Pore diameter distribution of SBA-15

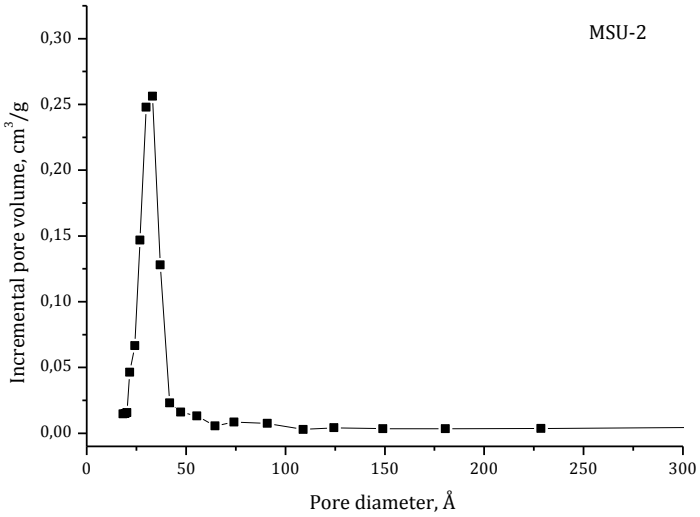

Fig. 15: Pore diameter distribution of MSU-2

On the other hand, alumina shows a very broad distribution between 100 and 1500 Å indicating no porosity in the mesoporous range (Figure 16).

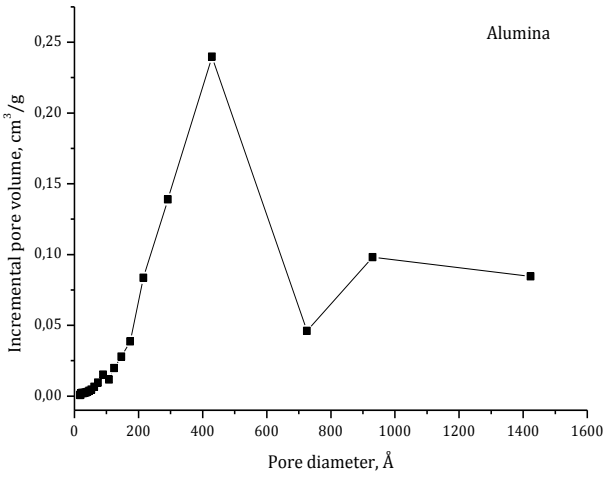

Fig. 16: Pore diameter distribution of alumina

In the case of the Pd-functionalized hybrid materials, all the N_2 adsorption-desorption isotherms are very similar to those of their parental materials. However, all the Pd-functionalized materials exhibited slightly lower surface areas and lower average pore volume compared to the parent material, as expected due to Pd deposition within the pores and/or on the surface of the materials, that may lead to a slight pore blocking and thus, to a detriment of their surface area and pore volume (See Tables 3 and 4). This phenomenon was especially notable when increasing the Pd loading in samples (See data of samples Pd 14-50 and Pd 15-20 in Tables 3 and 4, respectively. On the other hand, pore average diameter did not

remarkably change in the case of silica-based materials, while in the case of alumina, this parameter is not indicative due to its low porosity.

Table 3: Specific surface area, average pore diameter and pore volume of SBA-15 and Pd 14 series

Material	Specific surface area, m^2/g	Pore size, Å	Pore volume, cm^3/g
SBA-15	931	53.7	0.851
Pd 14-1	785	55.9	0.785
Pd 14-2	751	55.5	0.737
Pd 14-5	763	54.8	0.738
Pd 14-10	768	54.8	0.755
Pd 14-20	714	55.4	0.708
Pd 14-50	564	58.0	0.809

Table 4: Specific surface area, average pore diameter and pore volume of MSU-2 and Pd 15 series

Material	Specific surface area, m^2/g	Pore size, Å	Pore volume, cm^3/g
MSU-2	1052	31.2	1.055
Pd 15-1	970	32.5	0.990
Pd 15-2	863	30.8	0.874
Pd 15-5	979	32.3	0.989
Pd 15-10	896	31.6	0.901
Pd 15-15	934	32.2	0.943
Pd 15-20	919	31.7	0.936

Table 5: Specific surface area, average pore diameter and pore volume of alumina and AAL series

Material	Specific surface area, m^2/g	Pore size, Å	Pore volume, cm^3/g
Alumina	138	-	0.026
AAL20	121	-	-
AAL50	115	-	-

4.1.2. X-ray diffraction analysis (XRD)

SBA-15, MSU-2 and their corresponding Pd-functionalized analogues were characterized by low angle X-ray diffraction. Due to the fact that alumina and alumina supported materials are amorphous, they have not been characterized by low angle XRD.

The low angle XRD patterns of unmodified SBA-15 and MSU-2 are shown in Figures 17 and 18. Both materials exhibit a well resolved pattern, with two diffraction peaks at 0.95° (100) and 1.89° (110) for the SBA-15, and at 1.90° (100) and 3.46° (110) for the MSU-2. The observed XDR patterns are corresponding to a mesoscopic order attributed to mesoporous structure. Observing the diffraction peaks of the two materials it is clear that SBA-15 presents a more ordered structure than MSU-2, since it presents a lower peak broadening. In these structures, the d_{100} spacing, assigned to the pore-to-pore center correlation distance for each plane, was 92.20 and 46.43 Å for SBA-15 and MSU-2, respectively.

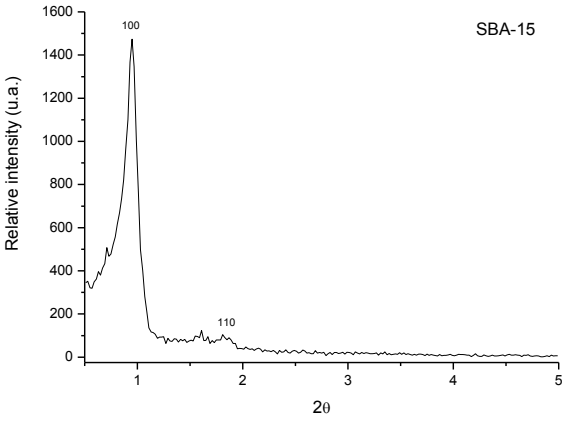

Fig. 17: XDR pattern for unmodified SBA-15

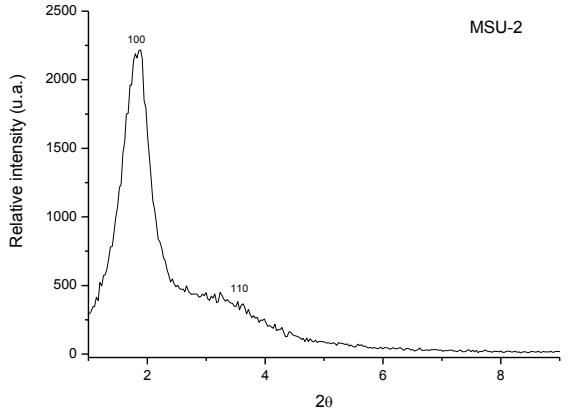

Fig. 18: XDR pattern for unmodified MSU-2

The XDR reflections observed for the loaded supports are similar to their non-loaded analogs (spectra not shown), with relatively small differences in the peak broadening and a slight decrease of their intensity due to a relatively small partial blocking of the dispersion centers as a consequence of the loading. This fact provides evidence that part of the loading process may occur inside the mesopore channels, since the attachment of metal nanoparticles or organic functional groups in the mesopore channels normally reduces the scattering power of the mesoporous silica walls.

Analyzing the data of the interplanar distances of all silica-based mesoporous materials, it is possible to calculate the average wall thickness of the studied materials, using the equation (2) (Pérez *et al*., 2009):

$$\text{Wall thickness} = \frac{2d_{100}}{\sqrt{3}} - \text{BHJ average pore diameter} \qquad (2)$$

The average wall thickness resulted to be 38.5 and 15.2 Å for unmodified SBA-15 and MSU-2, respectively. The wall thickness slightly increases after functionalization in the case of SBA-15 (with values from 38.6 to 40.2 Å), while it seems to be apparently constant in the case of MSU-2 functionalized materials (with vales from 14.6 to 15.9 Å). These results indicate that part of the Pd-nanoparticles may be located inside the pores of the corresponding materials.

For all the Pd-supported systems (SBA-15, MSU-2 and alumina-based hybrid materials) high angle X-ray diffractograms have been recorded in order to observe the peaks associated to palladium nanoparticles (Figure 19). Comparing the obtained diffractograms with others reported in the literature for Pd nanoparticles (Navaladian *et al*., 2008; Budarin *et al*., 2007) the assignation of the corresponding Miller indices was possible. Thus, most intense peaks at 2θ of 39.3, 45.4 and 67.5° were assigned to the (111), (200) and (220) planes, respectively, while the secondary peaks in intensity, at 80.3 and 84.6°, were assigned to the (311) and (222) planes, respectively.

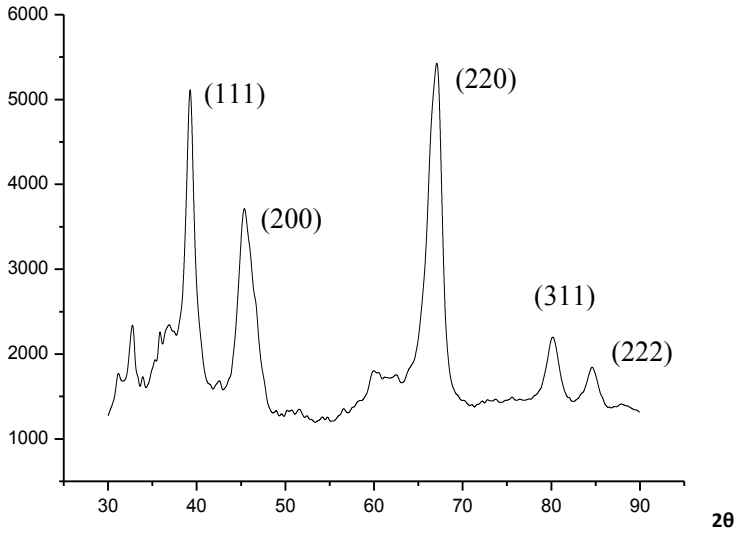

Fig. 19: High-angle XDR pattern of palladium nanoparticles-based materials

4.1.3. SEM analysis

All the synthesized materials have been characterized by Scanning Electronic Microscopy (SEM), in order to observe the morphology of the studied surfaces. There are no significant differences between the non-functionalized and the hybrid materials. The SBA-15-based materials showed uniform morphology of nanostructured rods (similar particle size of ca. 600 nm, Figure 20), while MSU-2 and its analogues show a similar spherical particle shape with similar mean diameter of between ca. 0.8 and 1.5 µM (Figure 21). Both types of silica-based materials have tendency to form cluster of aggregated particles.

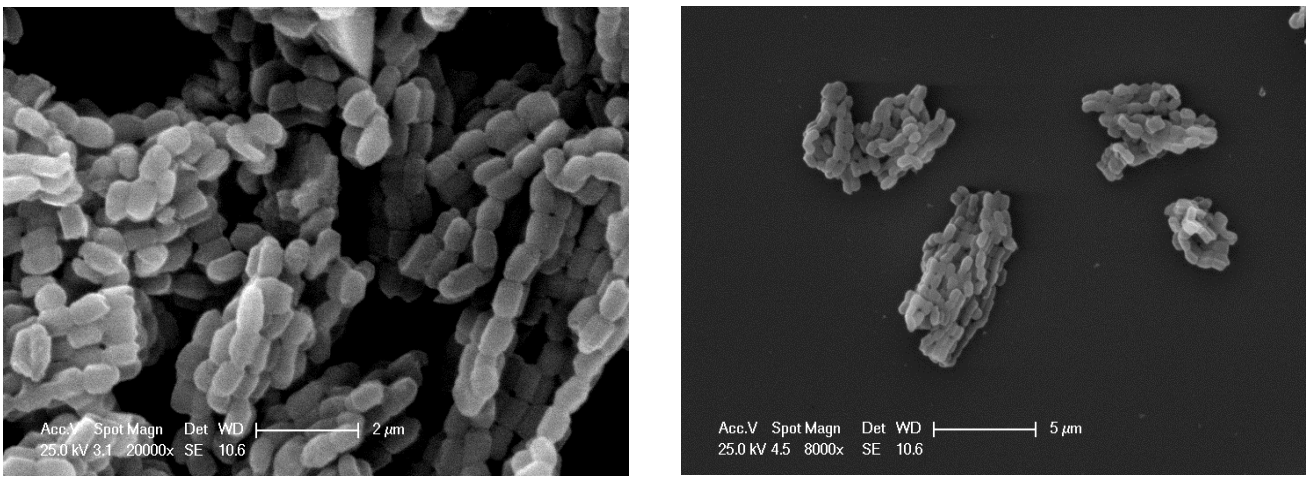

Fig. 20 SEM images of SBA-15 particles

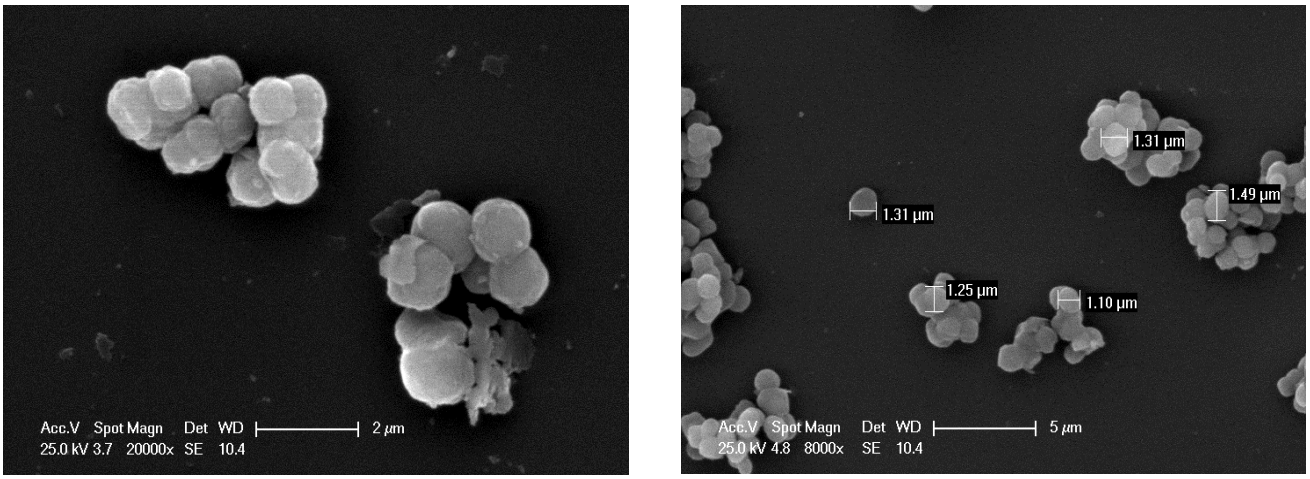

Fig. 21: SEM images of MSU-2 particles

On the other hand, alumina-based materials (Figure 22) can be considered as nanorods of up to 100 nm long (for further information see TEM pictures), although they aggregate in clusters of irregular shape and sizes.

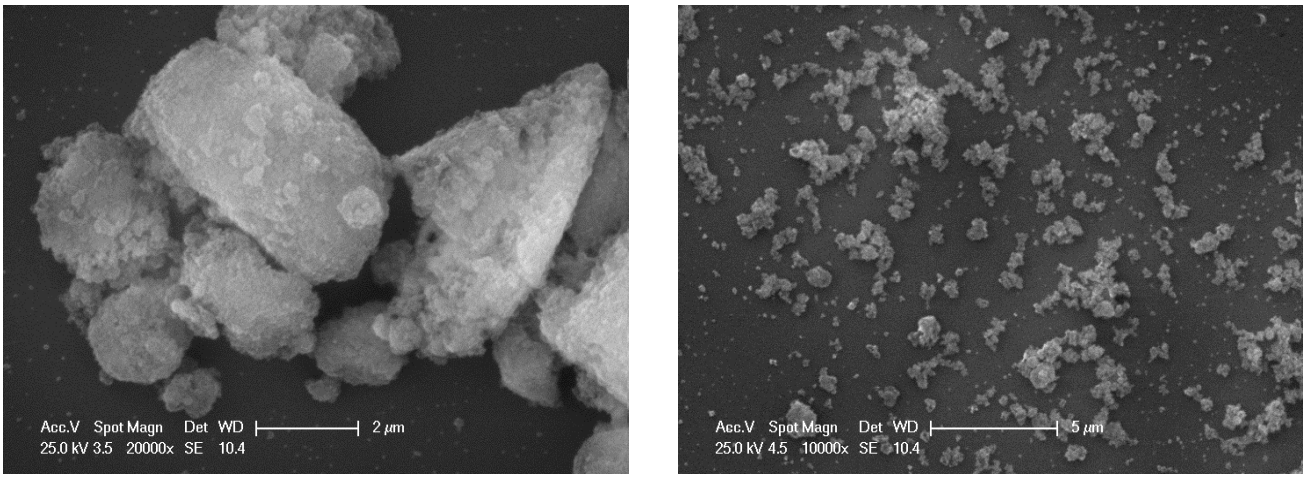

Fig. 22: SEM images of alumina particles

4.1.4. TEM analysis

All the bare supports have been characterized by Transmission Electronic Microscopy (TEM), in order to observe the morphology and arrangement of the pores. Figure 23 shows the transmission electron micrograph (TEM) images of SBA-15 silica which presents a highly ordered structure, with well-developed hexagonal porous parallel channels.

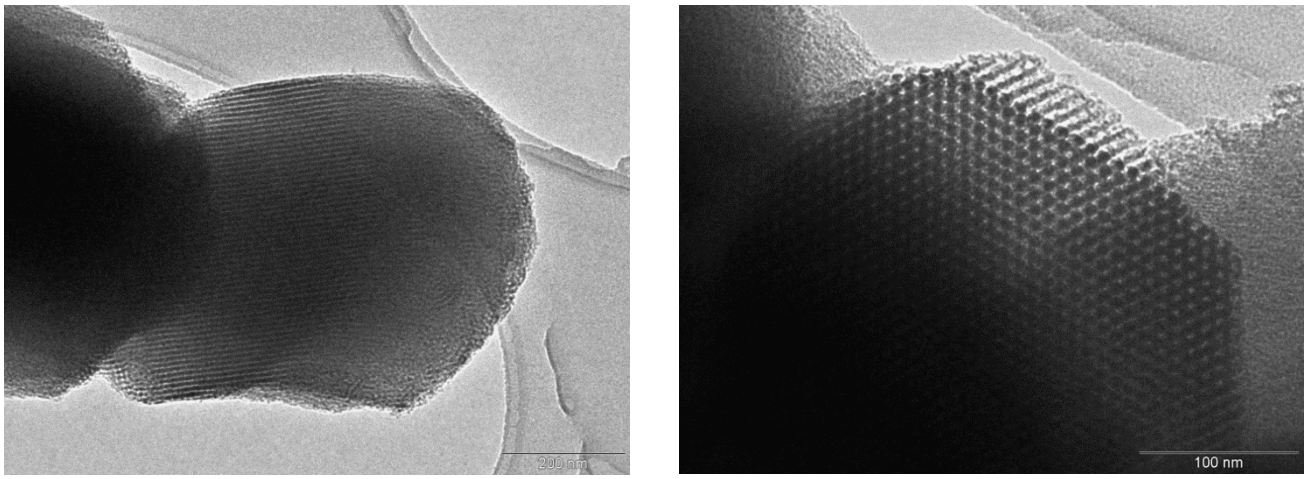

Fig. 23: TEM images of SBA-15 particles

In the case of MSU-2 system (Figure 24), the regular channel packaging order is loss, but it exhibits a 3D worm-hole porous framework with uniform channel pore.

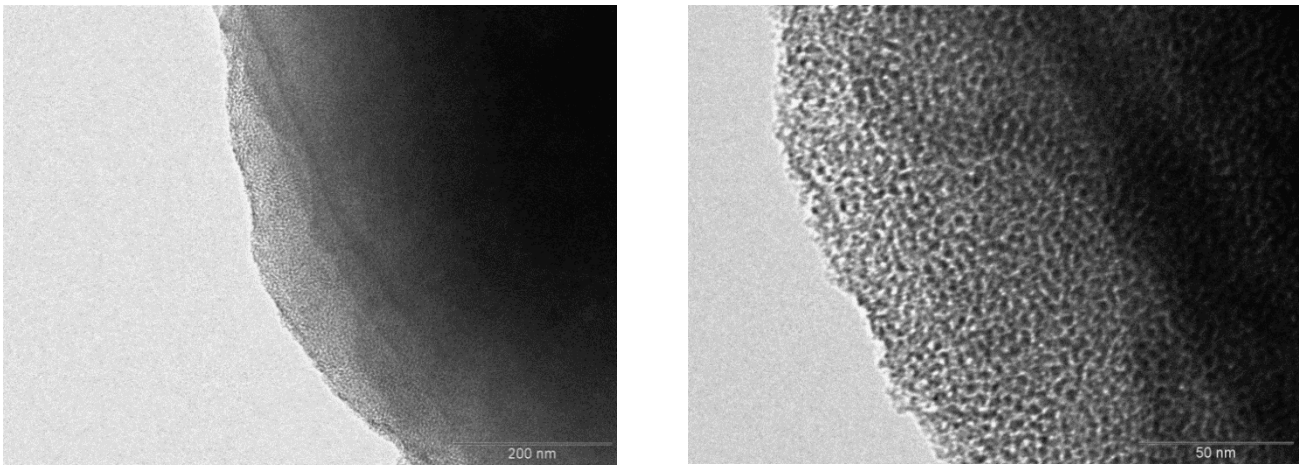

Fig. 24: TEM images of MSU-2 particles

In the case of alumina, the images provided by TEM (Figure 25) show that this material is composed by non-porous and non-crystalline nanorods of up to 100 nm long.

For the Pd-supported systems (Figures 26-28), show palladium nanoparticles as black dots either inside the pore of the mesoporous particles or fixed on the external surface of the support. All the systems show palladium nanoparticles with diameters ranging from ca. 5 to ca. 50 nm, although the larger particles seem to be clusters of very small nanoparticles. Palladium nanoparticles exhibit both spherical or slightly elongated shape, when they grew along the directions of channels.

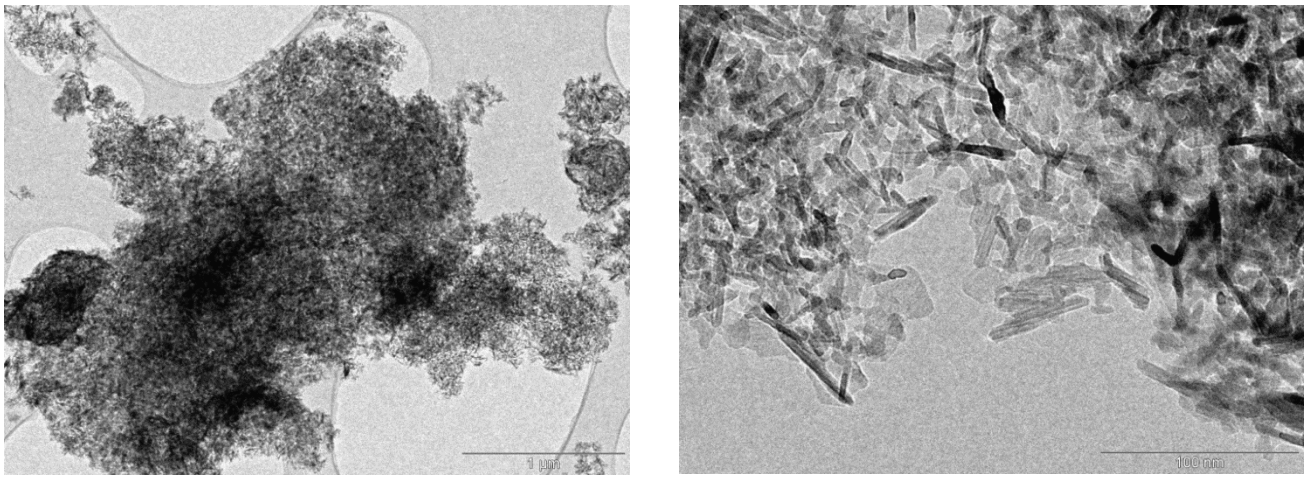

Fig. 25: TEM images of alumina particles

As observed in the following pictures, palladium nanoparticles show a very high tendency to aggregate on the surface of the mesoporous materials at higher loadings, resulting in a less homogeneous dispersion of the metal. The highly ordered structure of SBA-15 seems to promote a better incorporation of palladium nanoparticles within the mesoporous structure (Figure 26), as it was determined by the greater decrease in the specific surface area and pore volume, compared to MSU-2 (see data of N_2 adsorption-desorption analyses in Tables 3 and 4).

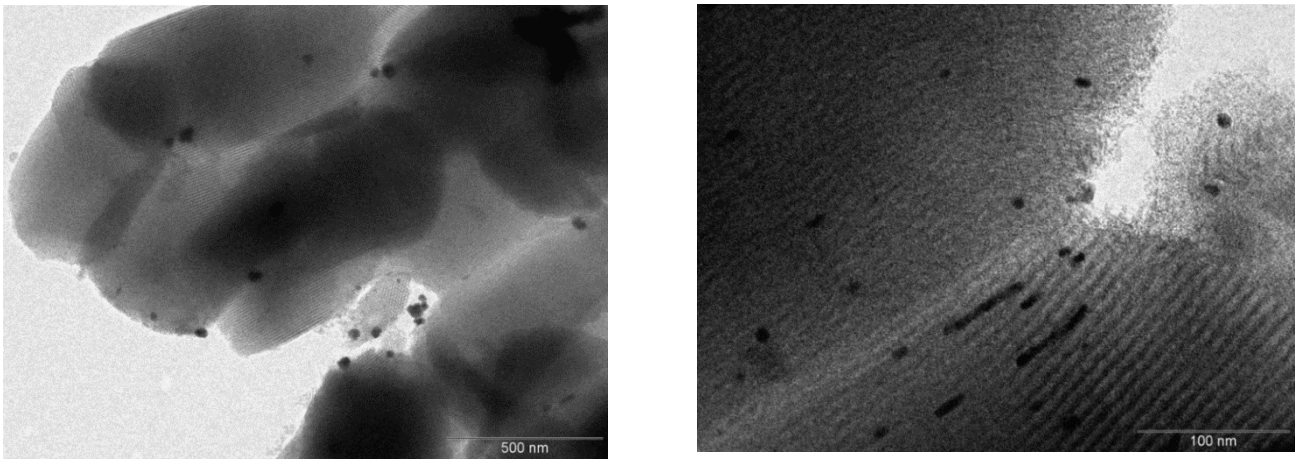

Fig. 26: TEM images of Pd 14 particles series

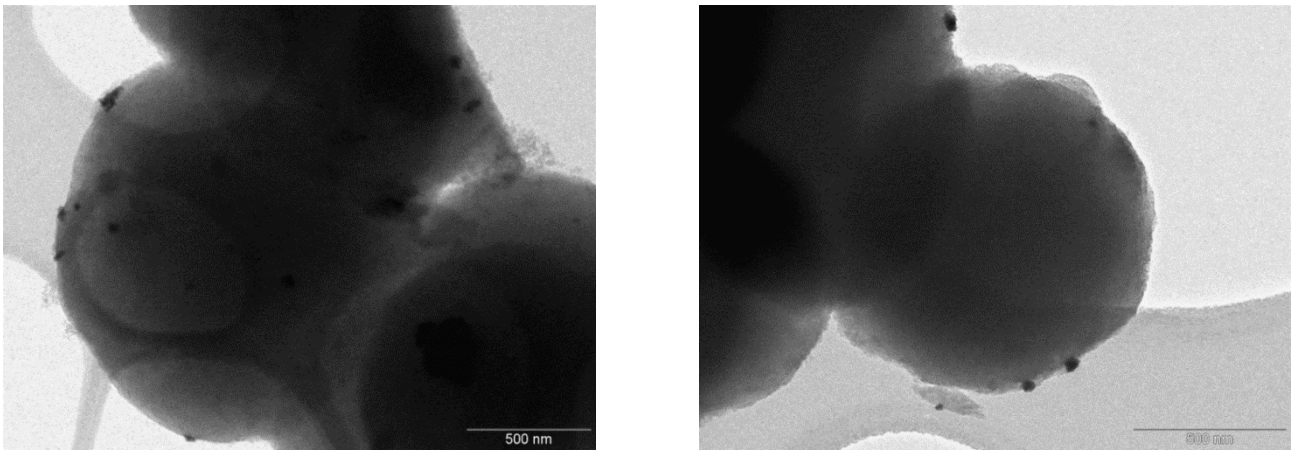

Fig. 27: TEM images of Pd 15 particles series

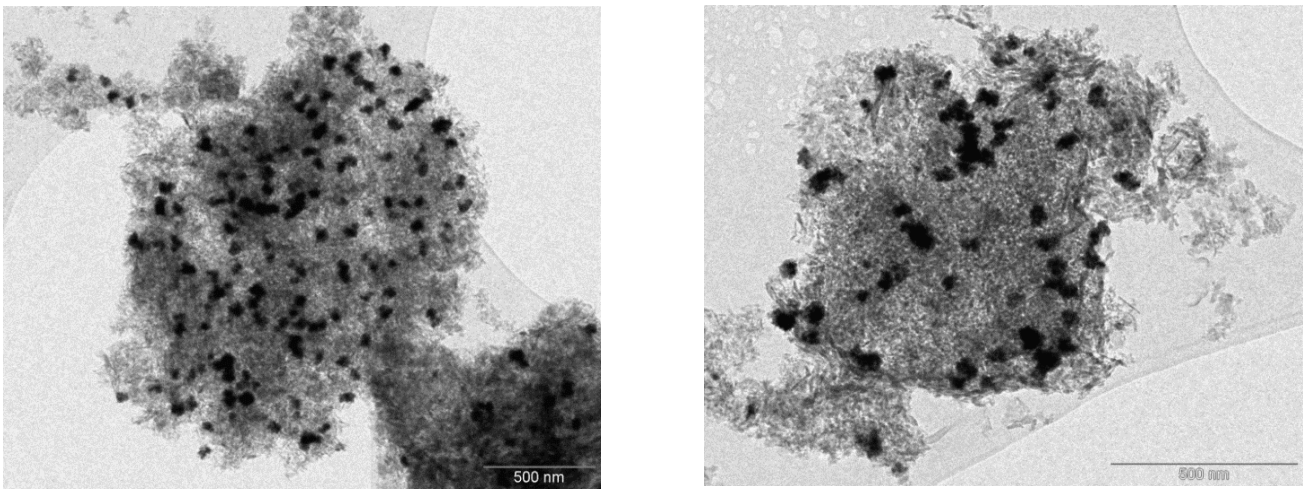

Fig. 28: TEM images of AAL particles series

4.1.6. X-ray fluorescence analysis (XRF): palladium loading analyses

X-ray fluorescence analysis was carried out to determine the quantity of embedded palladium in the final metal supported catalysts. A detailed study of the loading curves using different starting amounts of palladium precursor (1, 2, 5, 10, 20 and 50% wt. Pd) was performed in order to determine the amount of metal lost during the synthesis, and a possible saturation maximum of loading.

In the case of SBA-15, the maximum percentage of incorporated palladium is 12.8% wt.; which was obtained starting from 50 % wt. Pd. The data of all the experiments show a linear trend in the studied loading range. It seems to be unlikely that this linearity persists with higher percentages of starting palladium, although a maximum of saturation was not observed in the studied range (see Figure 29 and Table 6).

Table 6: Palladium loading on SBA-15

SBA-15		
Name	Theoretical Pd content (%)	Experimental Pd content (%)
Pd 14-1	1	0.39
Pd 14-2	2	0.54
Pd 14-5	5	1.20
Pd 14-10	10	2.10
Pd 14-20	20	6.11
Pd 14-50	50	12.8

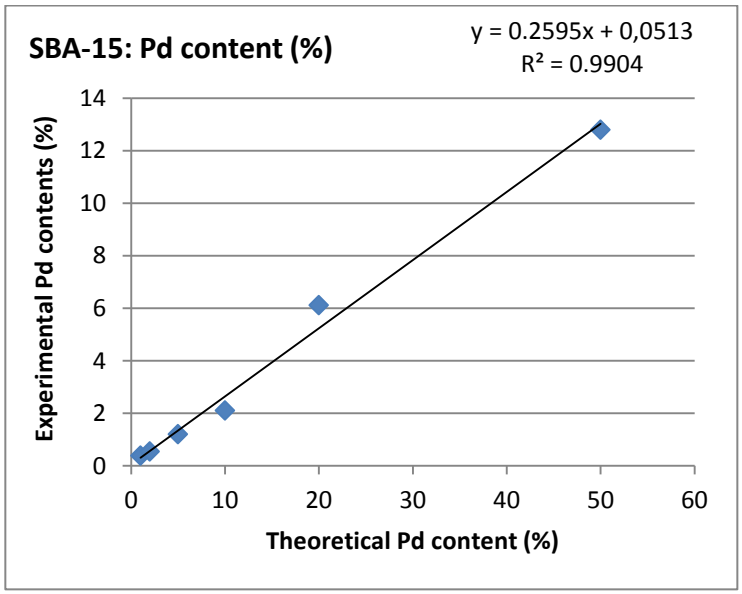

Fig. 29: Palladium loading plot on SBA-15

In the case of MSU-2, the maximum percentage of incorporated palladium is 4.46% wt. which was obtained starting from a 20 % wt. Pd. In this case, MSU-2 shows an exponential trend for the incorporation of palladium in the studied range (see Figure 30 and Table 7). Compared to SBA-15, the amount of incorporated palladium were generally lower, probably due to the smaller average pore diameter of MSU-2, even though this material (MSU-2) has a higher specific surface than SBA-15.

Table 7: Palladium loading on MSU-2

MSU-2		
Name	Theoretical Pd content (%)	Experimental Pd content (%)
Pd 15-1	1	0.63
Pd 15-2	2	0.48
Pd 15-5	5	0.70
Pd 15-10	10	1.12
Pd 15-15	15	2.18
Pd 15-20	20	4.46

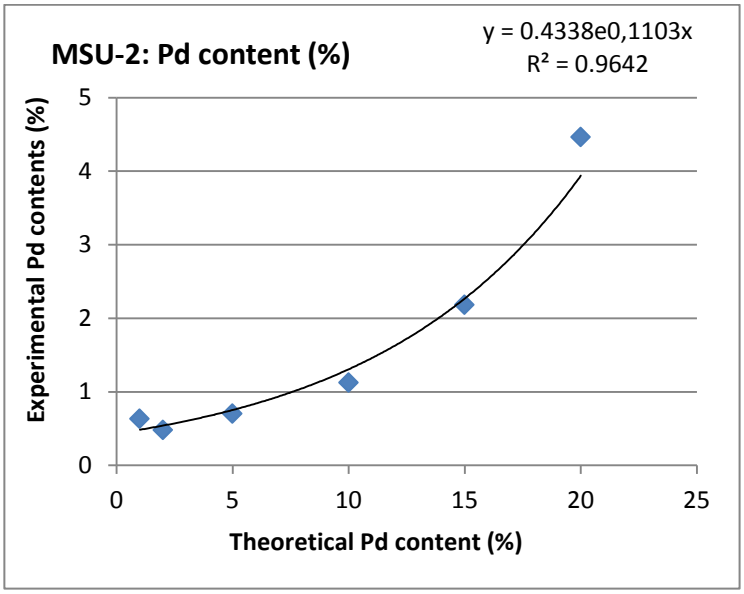

Fig. 30: Palladium loading plot on MSU-2

Finally, and compared to the other samples, alumina was the material that incorporated the highest amount of palladium nanoparticles, reaching up to 21.4 % wt. of Pd when starting from 50 % wt. Pd. The amorphous structure and the larger size of pores of alumina seem to positively affect the incorporation of the metal following a logarithmic tendency. Other possible explanation is a higher reducting nature of alumina compared to silica-based materials. Figure 31 and Table 8 show the corresponding loading results for Al_2O_3 surface.

Table 8: Palladium loading on alumina

Alumina		
Name	Theoretical Pd content (%)	Experimental Pd content (%)
AAL 1	1	1.27
AAL 2	2	2.65
AAL 5	5	5.27
AAL 10	10	8.54
AAL 20	20	9.25
AAL 50	50	21.4

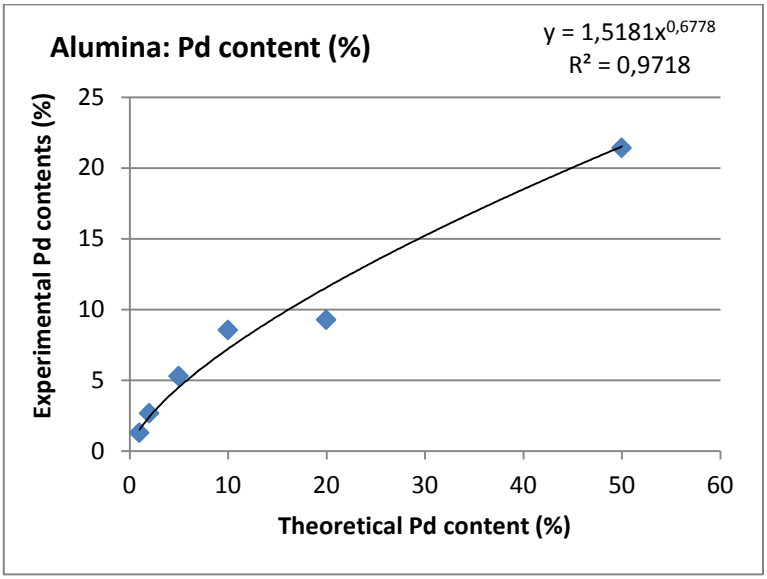

Fig. 31: Palladium loading plot on alumina

4.2. Catalytic tests

4.2.1. Preliminary tests

The catalytic activity of the Pd supported catalysts in S-M reactions was tested in two coupling reactions involving the same boronic acid and two different aromatic halides. For each reaction a test using a homogeneous commercial catalyst ($[Pd(PPh_3)_4]$ was carried out in order to compare the catalytic activity of the studied materials.

Reactions 1-8 (Tables 8 and 9) were carried out using reaction conditions already reported in literature (Trilla *et al*., 2008). Thus, a mixture DMF/H_2O (95/5) was used as solvent and K_2CO_3 as base, measuring the final conversion 24 hours after the beginning of the reaction.

Table 8 and 9 show the results obtained in the preliminary tests, for the reaction between 3-bromoanisole and 4-carboxyphenylboronic acid (Figure 32) and between 2-bromopyridine and 4-carboxyphenylboronic acid (Figure 33), respectively.

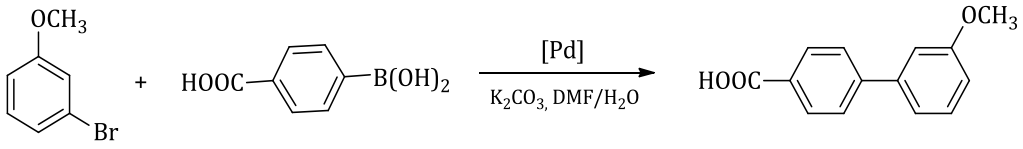

Fig 32: Reaction between 3-bromoanisole and 4-carboxyphenylboronic acid

Table 8: Data of the reactions 1-4 between 3-bromoanisole and 4-carboxyphenylboronic acid

Reaction	Catalyst	Temperature	Final Br conversion
1	Pd 14-20	110 °C	45 %
2	Pd 14-5	110 °C	15 %
3	Pd 14-5	70 °C	28.5 %
4	$[Pd(PPh_3)_4]$	110 °C	83.5 %

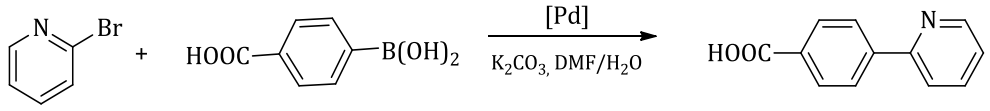

Fig. 33: reaction between 2-bromopyridine and 4-carboxyphenylboronic acid

Table 9: Data of the reaction 5-8 between 2-bromopyridine and 4-carboxyphenylboronic acid

Reaction	Catalyst	Temperature	Final Br conversion
5	Pd 15-20	110 °C	17 %
6	Pd 15-20	70 °C	33 %
7	Pd 14-20	70 °C	27.5 %
8	$[Pd(PPh_3)_4]$	110 °C	40 %

After the analysis of the results, we studied the influence of the temperature on the two reactions. Comparing reactions n° 2 and 3 and reactions n° 5 and 6, it seems clear that a decrease in temperature

from 110 °C to 70 °C has a remarkable influence on the final conversion of the halide compounds. In both cases a decrease in temperature led to conversions of halide of almost the half. This phenomenon suggests that temperatures higher than 70 °C may lead to some changes in the physical structure either of the catalysts or of the reactants which may affect the catalytic activity.

A subsequent study of the halide conversion at different range time in both reactions showed two different behaviors. While during the reaction n°4 between 3-bromoanisole and 4-carboxyphenylboronic acid, there is a rapid decrease of the concentration of the halide after the first 4 hours (followed by a slower decrease until the end of reaction time with a final conversion of 3-bromoanisole of 83.5 %), in the case of the reaction n°8 between 2-bromopyridine and 4-carboxyphenylboronic acid the concentration of the halide decreases more slowly and progressively during the reaction time, and does not seem to reach the minimum after 24 hours (with a final conversion of 2-bromopyridine of 40 %) (see Figure 34).

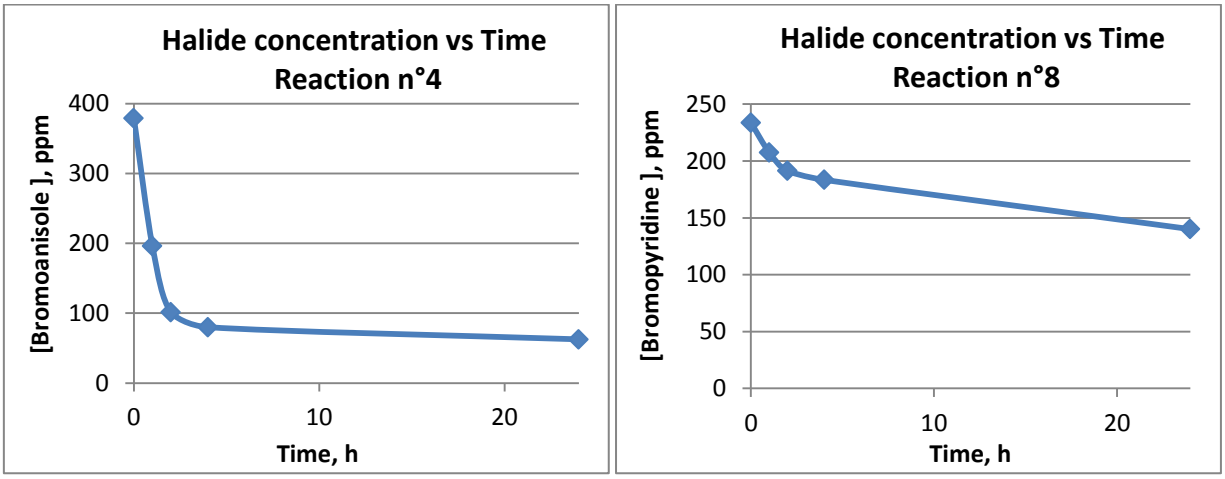

Fig. 34: Different kinetic behavior of the studied reactions

The differences in the conversion of both reactions seems to be justified by the fact that the *meta*-substituted arylbromides react faster than *ortho*-substituted derivatives (as is the case of 2-bromopyridine) due to sterical reasons. In addition, the inductive effect (-I) exerted by the methoxy group, which removes electron density, weakens the C-Br bond, increasing its reactivity. The reactivity of 2-bromopyridine seems to be lowered also by the conjugative effect, due to the electrons pair present at the nitrogen atom of the aromatic ring.

4.2.2. Detailed tests

With all the above results, we decided to study the catalytic activity of the catalysts focusing on the single reaction between 3-bromoanisole and 4-carboxyphenylboronic acid due to its higher conversion rates and selecting the reaction condition for these catalytic tests based on the previous results. These test were carried out at 70°C, in a solvent mixture DMF/H_2O (95/5) and using K_2CO_3 as the base. A reaction time

of 48 hours was chosen since after this time there was no further significant decrease in the concentration of 3-bromoanisole. The catalysts used for these tests are summarized in Table 10.

Table 10: Catalysts used in the detailed catalytic tests

Name	Support	Pd, %
AAL 50	Al_2O_3	21.40
AAL 20	Al_2O_3	9.25
Pd 14-50	SBA-15	12.80
Pd 15-15	MSU-2	2.18

The results of the tests using the studied materials as catalysts in the reaction between 3-bromoanisole and 4-carboxyphenylboronic acid and are shown in Figure 35.

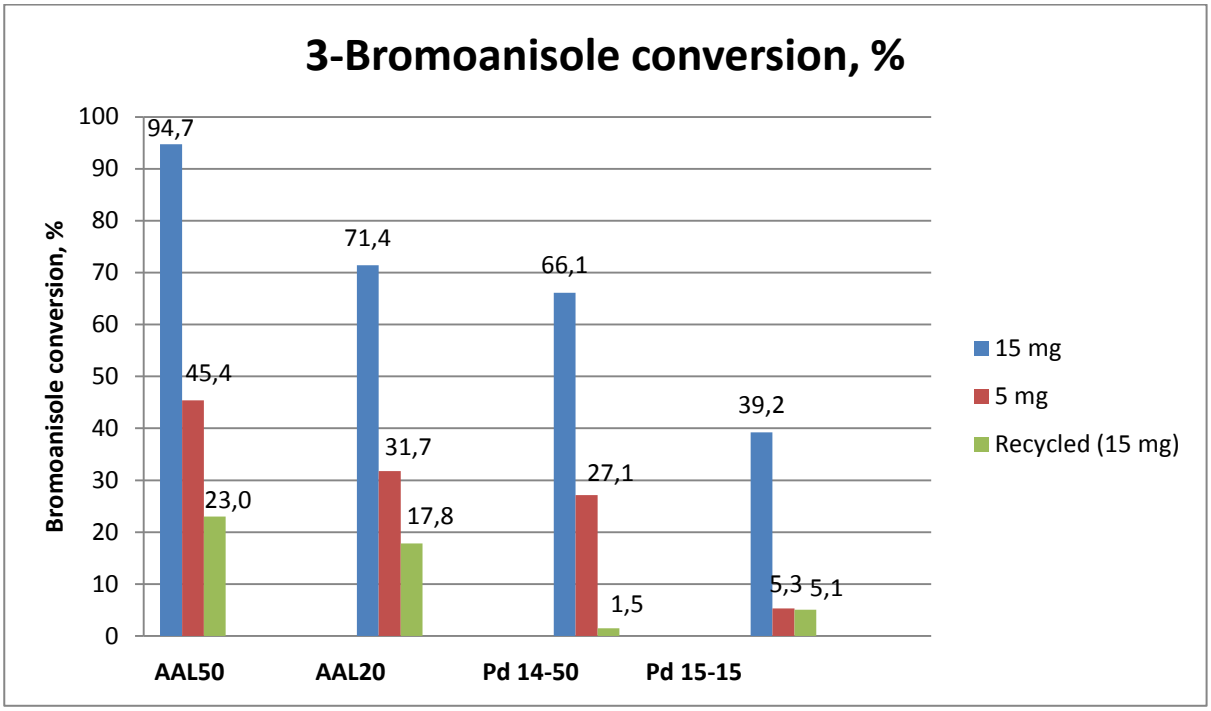

Fig. 35: Halide conversion in the reaction between 3-bromoanisole and 4-carboxyphenylboronic acid

The highest conversions were obtained with the catalyst AAL50, followed by AAL 20, Pd 14-50 and Pd 15-15.

This fact may be due to the following reasons:

- Palladium nanoparticles are more accessible in the alumina than in the other two surfaces, due to the non-porosity of the supporting material;

- The higher % wt. Pd in the AAL 50 catalyst, compared to AAL 20, Pd 14-50 and Pd 15-15.

The same tendency is clearly observed when using 5 mg of catalyst instead of 15 mg, however the obtained conversions are significantly lower indicating a high influence of the Pd content of the mixture on the halide conversion.

In the reusability tests a remarkable loss of activity of the catalysts has been observed after the first recycle test. This decrease is very high in the case of the silica-based catalysts Pd 14-50 and Pd 15-15 indicating the deactivation of the catalysts or leaching of the palladium nanoparticles after only a first cycle. On the other hand, the decrease in the activity is not so high in the case of the alumina-based catalysts AAL-50 and AAL-20, so that, we decided to further study in detail the reusability of the system based on AAL-50.

Thus, catalyst reusability was investigated using the same reaction conditions used in the conversion tests. Since the recovery of the catalyst in small quantities is very difficult, we designed experiments using higher amounts of catalyst but keeping the molar ratio of all the reactants and solvents. Figure 36 shows the results corresponding to six catalytic cycles using AAL-50

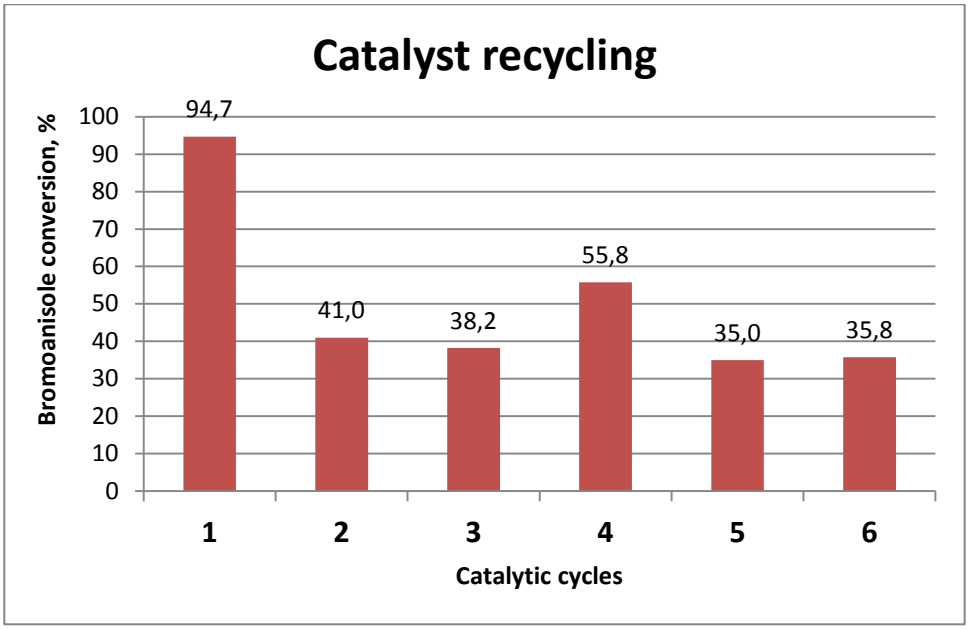

Fig. 36: Recycling test for AAL50 catalyst

A decrease of conversion after the first cycle (halide conversion of 95%) was observed, however, the conversion seems to be nearly constant (between 35-55%) for the subsequent four cycles, indicating a high degree of reusability of the catalysts under these conditions. These encouraging results need to be studied more in detail, but seem to be an interesting starting point for further catalytic investigations.

4.3. Cytotoxicity tests

As the catalytic study was mainly focused on the activity of the alumina-based materials, due to the very low reusability of the silica-based catalysts, the study of the cytotoxic activity has been focused on the bare silica (SBA-15 and MSU-2) and Pd-supported SBA-15 and MSU-2 (Pd 15-15 and Pd 14-50), in order to get new insights on the anticancer mechanism of this class of materials, which may be useful for the future preparation of bone fillings in patients with osteosarcomas or condroblastomas.

Thus, these materials have been analyzed in *in vitro* tests against malignant cells causing anaplasic thyroid carcinoma (8505C), head and neck tumor (A253), lung carcinoma (A549) and colon carcinoma (DLD-1). Cytotoxicity values, expressed as M_{50} values (the amount of material required to inhibit normal cell growth of the studied cell population by 50%), are collected in Table 11.

Table 11: M_{50} values of the studied materials

Cell line	SBA-15	MSU-2	Pd 14-50	Pd 15-15
8505C	>1500	387.2 ± 2.7	110.6 ± 19.7	417.1 ± 25.9
A253	>1500	229.1 ± 2.1	109.5 ± 16.1	283.5 ± 13.5
A549	>1500	442.0 ± 20.4	238.5 ± 19.6	553.4 ± 12.8
A2780	>1500	217.4 ± 8.4	206.7 ± 20.7	256.9 ± 15.4
DLD-1	>1500	205.4 ± 6.5	154.7 ± 5.92	241.2 ± 17.8

All the materials show a dose-dependent cytotoxicity (Figure 37) against all the studied cancer cells, except SBA-15 which showed no activity in the studied range (M_{50} > 1500 μg, data not shown in Figure 37).

Considering that the SBA-15-based material Pd 14-50 shows a relatively high cytotoxicity, it seems that palladium nanoparticles have a positive influence on the anticancer activity; nevertheless, Pd 15-15 has shown a lower cytotoxic activity compared to the corresponding non-functionalized surface MSU-2. These contradictory results may be explained by the fact that Pd content needs to reach a minimum to have a remarkable influence on the cytotoxic action. In this context, Pd 14-50 (12.8% wt. Pd) shows a higher cytotoxic activity than Pd 15-15 (2.18% wt. Pd), which may indicate that palladium content is essential for a substantial increase of the cytotoxic activity.

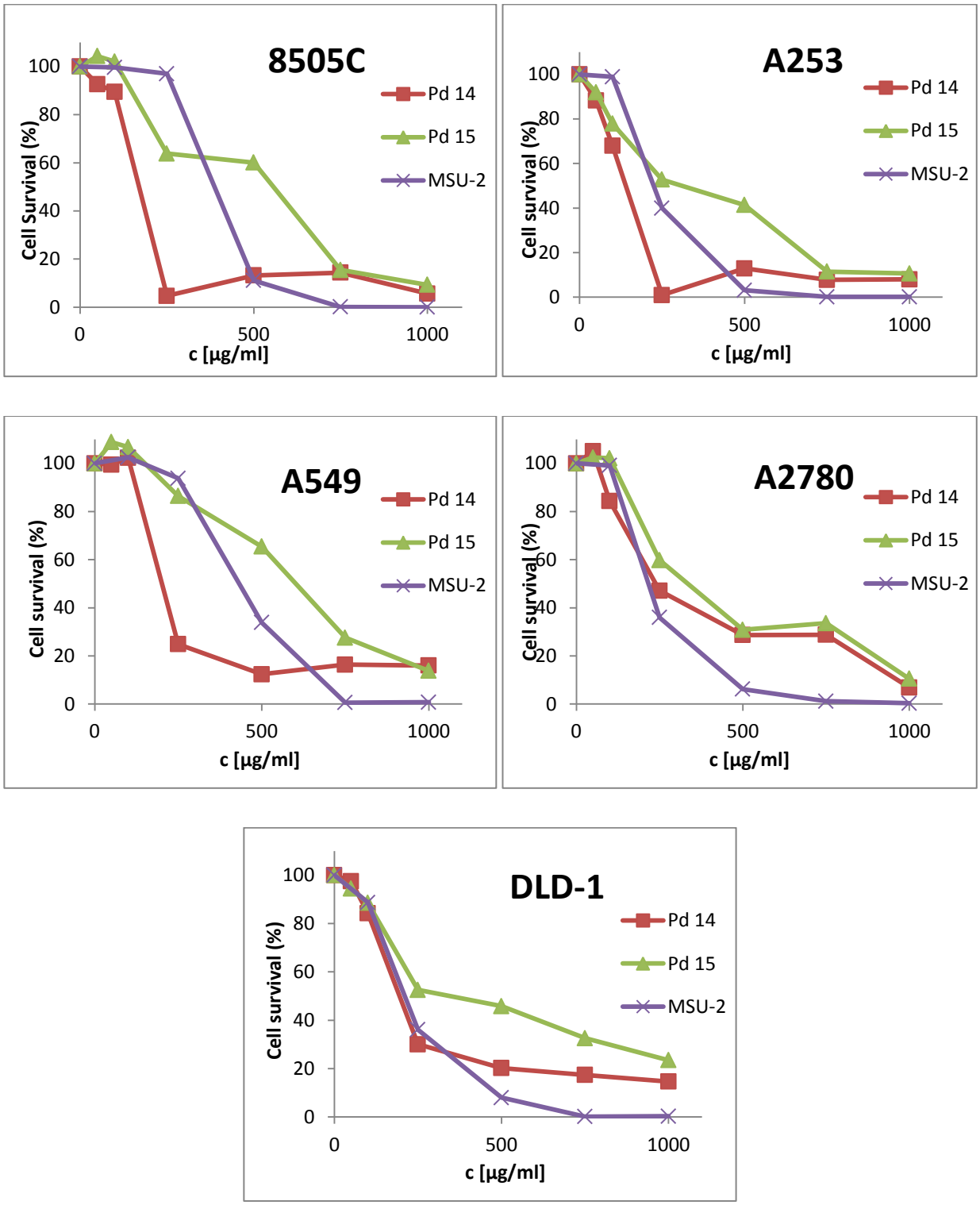

Fig. 37: Graphs show cell survival vs. surface concentration for different cancer cell lines

Comparing the obtained results, it seems risky to further comment on tendencies of the cytotoxic nature of these materials which seems to depend on the amount of employed material, palladium amount in the material, studied cell type and surface type. However, this is the first report about the cytotoxic activity of supported palladium nanoparticles and further studies in the field should be carried out in order to determine whether this kind of materials can be used for biological purposes.

5. Conclusions

The main conclusions of the work reported in this project are:

1. Supported palladium nanoparticles have been synthesized using the following supports: Al_2O_3, SBA-15 and MSU-2. The loading procedure show different tendencies for the incorporation of the metal nanoparticles depending on the supporting material. The maximum percentage of impregnated Pd nanoparticles on these surfaces was of 21.4% wt. on Al_2O_3, 12.8% wt. on SBA-15 and 4.46% wt. on MSU-2.
2. The non-modified materials and the Pd-functionalized materials have been characterized by different analytical techniques: nitrogen physisorption (BET), X-ray diffraction (XRD), X-ray fluorescence (XRF), scanning electron microscopy (SEM) and transmission electron microscopy (TEM) observing that the functionalization of the materials with palladium nanoparticles took place.
3. The obtained systems have been used as catalysts for the Suzuki-Miyaura (SM) coupling reaction between 3-bromoanisole and 4-carboxyphenylboronic acid and the reaction between 2-bromopyridine and 4-carboxyphenylboronic acid. Maintaining the same reaction conditions a higher catalytic activity was observed at 70°C compared to 110°C.
4. The reaction between 3-bromoanisole and 4-carboxyphenylboronic acid catalyzed by the systems reported here and the reference catalyst $[Pd(PPh_3)_4]$ is faster with both heterogeneous and homogeneous catalysts (needs only 24 hours for the maximum conversion) than that of 2-bromopyridine and 4-carboxyphenylboronic acid (which needs around 48 hours) maybe due either to sterical and electronic reasons.
5. In the reaction between 3-bromoanisole and 4-carboxyphenylboronic acid catalyzed by AAL 50, AAL 20, Pd 14-50 and Pd 15-15, conversion of the halide compound was quantified using 15 mg or 5 mg of fresh catalyst and 15 mg of recycled catalyst, observing that the highest conversions were obtained with the catalyst AAL 50, followed by AAL 20, Pd 14-50 and Pd 15-15 indicating a possible influence of the palladium amount on the final catalytic activity.
6. In the reaction between 3-bromoanisole and 4-carboxyphenylboronic acid catalyzed by AAL 50, AAL 20, Pd 14-50 and Pd 15-15, the conversions using 15 mg of catalyst are higher than those obtained with 5 mg, indicating an influence of the palladium amount on the final catalytic activity.
7. A reusability study of AAL50 in up to six catalytic cycles was carried out observing that the conversion of the halide is reduced from 95% (in the first cycle) to 35-55% after the first catalytic cycle, however, it remains nearly constant for the other five cycles indicating a high degree of recyclability of the material.

8. Pd 15-15 and Pd 14-50 catalysts and MSU-2 and SBA-15 supports have been tested *in vitro* against human cancer cells; observing that in the case of surface Pd 14-50 the activity is higher than the not functionalized SBA-15, while Pd 15-15 shows a lower cytotoxic acitivity than MSU-2. Thus, no correlations between materials and cytotoxicity were observed, because the cytotoxic nature of these materials seems to depend on the amount of employed material, palladium amount in the material, studied cell type and surface type.

6. References

- S. Abu-Surrah, T. A. Al-Allaf, L. J. Rashan, M. Klinga, M. Leskela; **Synthesis, crystal structure and initial biological evaluation of the new enantiomerically pure chiral palladium(II) complex trans-bis{endo-(1R)-1,7,7-trimethylbicyclo[2.2.1]- heptan-2-amino}palladium(II)dichloride**. *European Journal of Medicinal Chemistry*, 2002, 27, 919-922.
- S. Abu-Surrah, K. A. Abu Safieh, I. M. Ahmadb, M. I. Abdalla, M. T. Ayoub, A. K. Qaroush, A. M. Abu-Mahtheieh; **New palladium(II) complexes bearing pyrazole-based Schiff base ligands: Synthesis, characterization and cytotoxicity**. *European Journal of Medicinal Chemistry*, 2010, 45, 474-475.
- A. Balbín Caminero; **Estudio de las propiedades catalíticas y antitumorales de nanopartículas de paladio soportadas**. *Supervisors: S. Gómez-Ruiz, J. Ceballos Torres*, Final Year Project, Universidad Rey Juan Carlos, 2012.
- V. Barau, A. Budarin, R. Caragheorgheopol, D. J. Luque, A. Macquarrie, V. S. Prelle, M. Teodorescu, A. Zaharescu; **A Simple and Efficient Route to Active and Dispersed Silica Supported Palladium Nanoparticles**. *Catalysis Letters*, 2008, 124, 204-214.
- R. B. Bedford, U. G. Singh, R. I. Walton, R. T. Williams, S. A. Davis; **Nanoparticulate Palladium Supported by Covalently Modified Silicas: Synthesis, Characterization, and Application as Catalysts for the Suzuki Coupling of Aryl Halides**. *Chemistry of Materials*, 2005, 17, 701-707.
- T. Borkowski, A.M. Trzeciak, W. Bukowski, A. Bukowska, W. Tylus, L. Kępinski; **Palladium(0) nanoparticles formed *in situ* in the Suzuki-Miyaura reaction: the effect of a palladium(II) precursor**. *Applied Catalysis A: General*, 2010, 378, 83-89.
- V. Budarin, J. H. Clark, R. Luque, J. Macquarrie, J. Robin, R. White; **Palladium nanoparticles on polysaccharide-derived mesoporous materials and their catalytic performance in C–C coupling reactions**, *Green Chemistry*, 2008, 10, 382-387.
- Y. Chun, J. Bao, J. L. Jin, C. Jie, H. Qin, P. Zheng; **Catalytic oxidation of benzyl alcohol on Au or Au–Pd nanoparticles confined in mesoporous silica**. *Applied Catalysis B: Environmental*, 2009, 92, 202-208.
- A. García-Peñas, S. Gómez-Ruiz, D. Pérez-Quintanilla, R. Paschke, I. Sierra, S. Prashar, I. del Hierro, G. N. Kaluđerović; **Study of the cytotoxicity and particle action in human cancer cells of titanocene-functionalized materials with potential application against tumors**. *Journal of Inorganic Biochemistry,* 2012, 106, 100-110.
- Z. Hou, N. Theyssen, A. Brinkmann, K. V. Klementiev, W. Grünert, M. Bühl, W. Schmidt, B. Spliethoff, B. Tesche, C. Weidenthaler, W. Leitner; **Supported palladium nanoparticles on hybrid mesoporous silica: Structure/activity-relationship in the aerobic alcohol oxidation using supercritical carbon dioxide**. *Journal of Catalysis* 2008, 258, 315 – 323.

- N. Jamwal, M. Gupta, S. Paul; **Hydroxyapatite-supported palladium (0) as a highly efficient catalyst for the Suzuki coupling and aerobic oxidation of benzyl alcohols in water**. *Green Chemistry,* 2008, 10, 999 – 1003.
- L. Jiao, J. R. Regalbuto; **The synthesis of highly dispersed noble and base metals on silica via strong electrostatic adsorption: II. Mesoporous silica SBA-15**. *Journal of Catalysis,* 2008, 260, 342-350.
- G. N. Kaluđerović, D. Pérez-Quintanilla, Ž. Žižak, Z. D. Juranić, S. Gómez-Ruiz; **Improvement of cytotoxicity of titanocene-functionalized mesoporous materials by the increase of the titanium content**. *Dalton Transactions,* 2010, 39, 2597–2608.
- J. Karimi, S. Abedi, J. H. Clark, V. Budarin; **Highly efficient aerobic oxidation of alcohols using a recoverable catalyst: the role of mesoporous channels of SBA-15 in stabilizing palladium nanoparticles**. *Angewandte Chemie,* 2006, 45, 4776–4779.
- C. Li, Q. Zhang, Y. Wang, H. Wan; **Preparation, characterization and catalytic activity of palladium nanoparticles encapsulated in SBA-15**. *Catalysis Letters*, 2008, 120, 126–136.
- Y.Ma, B. J. Dou, J. J. Li, J. Cheng, Q. Hu, Z. P. Hao, S. Z. Qiao; **Catalytic oxidation of benzyl alcohol on Au or Au–Pd nanoparticles confined in mesoporous silica**. *Applied Catalysis B: Environmental*, 2009, 92, 202–208.
- S. MacQuarrie, B. Nohair, J. Hugh Horton, S. Kaliaguine, C. M. Crudden; **Functionalized mesostructured silicas as supports for palladium catalysts: effect of pore structure and collapse on catalytic activity in the Suzuki-Miyaura reaction**. *The Journal of Physical Chemistry C*, 2010, 114, 57–64.
- M. Manzano, M. Vallet-Regí; **New developments in ordered mesoporous materials for drug delivery**. *Journal of Materials Chemistry*, 2010, 20, 5593–5604.
- Á. Mastalir, B. Rác, Z. Király, Á. Molnár; **In situ generation of Pd nanoparticles in MCM-41 and catalytic applications in liquid-phase alkyne hydrogenations**. *Journal of Molecular Catalysis A: Chemical,* 2007, 264, 170–178.
- S. Navaladian, B. Viswanathan, T. K. Varadarajan, R. P. Viswanath; **A rapid synthesis of oriented palladium nanoparticles by UV irradiation**. *Nanoscale Res Lett*, 2009, 4, 181–186.
- J. N. Park, A. J. Forman, W. Tang, J. Cheng, Y. S. Hu, H. Lin, E. W. McFarland; **Highly active and sinter-resistant Pd-nanoparticle catalysts encapsulated in silica**. *Small*, 2008, 10, 1694–1697.
- D. Pérez-Quintanilla, S. Gómez-Ruiz, Ž. Žižak, I. Sierra, S. Prashar, I. del Hierro, Mariano Fajardo, Z. D. Juranić, G. N. Kaluđerović; **A new generation of anticancer drugs: mesoporous materials modified with titanocene complexes**. *Chemistry,* 2009, 15, 5588–5597.
- J. A. Pérez de Haro; **Estudio del autoacoplamiento de ácido fenilborónico catalizado por complejos ortometalados de paladio**. *Supervisors: J. L. Serrano Martínez, L. G. González*, Final Year Project, Universidad Politécnica de Cartagena, 2010.

- S. Sánchez-Muñoz, S. Gómez-Ruiz, D. Pérez-Quintanilla, S. Morante-Zarcero, I. Sierra, S. Prashar, R. Paschke, G. N. Kaluđerović; **Preliminary Study of the Anticancer Applications of Mesoporous Materials functionalized with the Natural Product Betulinic Acid**. *ChemMedChem*, 2012, 7, 670-679.
- P. Skehan, R. Storeng, D. Scudiero, A. Monks, J. McMahon, D. Vistica, J. T. Warren, H. Bokesch, S. Kenney, M. R. Boyd; **New colorimetric cytotoxicity assay for anticancer-drug screening**. *Journal of the National Cancer Institute*, 1990, 82, 1107-1112.
- I. Slowing, J. L. Vivero-Escoto, B. G. Trewyn, V. S.-Y. Lin; **Mesoporous silica nanoparticles: structural design and applications**. *Journal of Materials Chemistry*, 2010, 20, 7924-7937.
- M. Trilla, G. Borja, R. Pleixats, M. Wong Chi Man, C. Bied, J. E. Moreau; **Recoverable palladium catalysts for Suzuki–Miyaura cross-coupling reactions based on organic-inorganic hybrid silica materials containing imidazolium and dihydroimidazolium salts**. *Advanced Synthesis and Catalysis,* 2008, 350, 2566-2574.
- R. Xing, Y. Liu, H. Wu, X. Li, M. He, P. Wu; **Preparation of active and robust palladium nanoparticle catalysts stabilized by diamine-functionalized mesoporous polymers**. *Chemical Communications,* 2008, 6297-6299.
- I. Yuranov, P. Moeckli, E. Suvorova, P. Buffat, L. Kiwi-Minsker, A. Renkena; **Pd/SiO_2 catalysts: synthesis of Pd nanoparticles with the controlled size in mesoporous silicas**. *Journal of Molecular Catalysis A: Chemical*, 2003, 192, 239-251.